U. of Iowa 88-13

WAVE-PARTICLE INTERACTIONS IN THE MAGNETOSPHERE OF URANUS

by

W. S. Kurth,[1] D. A. Gurnett,[1] F. L. Scarf,[2]

and F. V. Coroniti[3]

July 1988

[1]Department of Physics and Astronomy
The University of Iowa
Iowa City, Iowa 52242

[2]TRW Space and Technology Group
One Space Park
Redondo Beach, California 90278

[3]Department of Astronomy and
Department of Physics
University of California
Los Angeles, California 90028

The research at the University of Iowa was supported by National Aeronautics and Space Administration through Contract 957723 with the Jet Propulsion Laboratory. The research at TRW was supported by National Aeronautics and Space Administration through Contract 957805 with the Jet Propulsion Laboratory.

ABSTRACT

The Voyager 2 encounter of Uranus has provided observations of plasma waves in and near the magnetosphere. These data, while the first from Uranus, will also be the only direct information on wave-particle interactions at this planet for many years to come. The observations include electrostatic waves upstream of the bow shock, turbulence in the shock, Bernstein emissions and whistler mode waves in the magnetosphere, broadband electrostatic noise in the magnetotail, and a number of other types of plasma waves which have yet to be clearly identified. Each of these types of waves exist in a plasma environment which both supports the growth of the waves and is modified by interactions with the waves. Wave-particle interactions provide the channels through which the waves can accelerate, scatter, or thermalize the plasmas. The most spectacular example in the case of Uranus is the extremely intense whistler mode activity in the inner magnetosphere which is the source of strong pitch angle diffusion. The resulting electron precipitation is sufficient to produce the auroral emissions observed by Voyager. The strong diffusion, however, presents the problem of supplying electrons in the range 5 - 40 keV in order to support the losses to the atmosphere.

1. INTRODUCTION

The magnetosphere of Uranus is the site of intense plasma wave activity (Gurnett et al., 1986) and exhibits evidence of strong wave-particle interactions important in the generation of the aurora observed by the Voyager ultraviolet sensor (UVS) and in the energy budget of the magnetosphere. The magnetosphere is also the site of a number of weaker plasma waves which interact with the local plasma, but which are of lesser importance in the overall dynamics of the system. In this chapter we will review the observations of plasma waves and instabilities observed by the Voyager plasma wave receiver in and near the Uranian magnetosphere. We will attempt to assess the impact of the observed plasma waves on the plasma and energetic particle populations resident in the various regions of the magnetosphere. Finally, we will try to understand the role of the waves in the various magnetospheric processes.

The Uranian magnetosphere comprises the Uranian magnetic field (Ness et al., 1986; Ness et al., this volume) and a thermal plasma and various energetic particle populations composed almost exclusively of protons (Bridge et al., 1986; Belcher et al., this volume; Krimigis et al., 1986; Cheng et al., this volume; Stone et al., 1986). The outer boundary of the magnetosphere, the magnetopause, was crossed by Voyager 2 at a distance of about 18 R_U on the dayside of Uranus with the bow shock being detected at a distance of about 23.7 R_U. The highly asymmetric pressure of the supersonically flowing solar wind is responsible for the formation of a long magnetic tail, similar to the

case in other magnetospheres. The trajectory of Voyager 2 was not specifically designed to traverse the tail to any great distance; nevertheless, it left the dawn flank of the tail at a distance of about 80.5 R_U from Uranus. One of the most spectacular discoveries of the Voyager flyby of Uranus was the ~60° tilt of the magnetic dipole with respect to the rotational axis as well as an offset of nearly a third of a planetary radius (Ness et al., 1986). This unexpected field configuration dismantled earlier speculations on the form of the Uranian magnetosphere (c.f. Siscoe, 1975; Hill, 1984). The unusual dipole configuration leads to many asymmetries in the magnetosphere, one of the most obvious being the highly asymmetric radio emission pattern (Warwick et al., 1986; Kaiser et al., 1987; Desch et al., this volume) and the resulting implication that the plasma populations responsible for driving the radio emissions find suitable conditions for existence on the nightside, southern magnetic hemisphere.

Figure 1 provides an overview of the Uranus encounter as viewed by the plasma wave spectrum analyzer from before the inbound bow shock to the first encounters of the bow shock on the outbound leg of the trajectory (Gurnett et al., 1986). Upstream wave activity and the bow shock signature can be seen early on January 24 and these waves will be discussed in Section 2. Little wave activity is seen after the shock crossing until shortly after noon on January 24 when Bernstein emissions are observed in the 1.0- and 1.78-kHz channels at about 1300 SCET. Other Bernstein wave activity can be found closer to Uranus, above the electron cyclotron frequency f_c contour which is based on

the intensity of the magnetic field provided by the OTD magnetic field model (Ness et al., 1986) by f_c [Hz] = 28|B| [nT]. The Bernstein emissions will be discussed in Section 3. As in the case of the other planetary magnetospheres (Kurth, 1985), the bulk of the plasma wave activity is found in the inner magnetosphere, from about 1500 through 2100 SCET on the same day, and is located below the f_c contour. A comparison with the plasma and energetic particle observations (Belcher et al., this volume; Cheng et al., this volume) would verify that this is the same interval when plasma and energetic particle fluxes were high. This band of wave activity, which happens to be the most intense whistler-mode activity observed thus far in the outer planets' magnetospheres (Gurnett et al., 1986; Scarf et al., 1987) will be discussed fully in Section 4, specifically with regard to the potential for strong pitch-angle scattering provided by these waves. Finally, some weak activity can be found during the magnetotail traversal after about 2200 SCET on January 24 below about 100 Hz. These waves, tentatively identified as broadband electrostatic noise, will be discussed in Section 5.

Throughout this chapter, reference will be made to the Voyager 2 plasma wave receiver. While it is inappropriate to describe this instrument in great detail, here, it is important to understand that it is composed of two sections. The primary section for the results presented herein is the 16-channel spectrum analyzer which returns an amplitude in each of 16 fixed-frequency channels logarithmically spaced in frequency from 10 Hz to 56.2 kHz every 4 seconds. The other section is a wideband waveform receiver which returns a digitized sample of the waveform in the frequency range of about 40 Hz to 12 kHz

in a continuous fashion for periods of time of either 10 or 48 seconds. Because this section of the instrument requires a data rate of 115 kbps, only short snapshots can be afforded at infrequent intervals. However, these snapshots provide extremely high temporal and spectral resolution and greatly enhance our capability to identify various wave emissions. Finally, the Voyager plasma wave receiver has only the shared use of the planetary radio astronomy antennas for sensors, which it uses as a balanced dipole with an effective length of 7.07 m. Hence, any identification of an emission as electrostatic or electromagnetic can be made only on the basis of the frequency of the emission with respect to critical frequencies of the plasma, the spectral and temporal variations of the emission (electrostatic waves tend to be burstier than electromagnetic waves), and by analogy with similar emissions observed in the terrestrial magnetosphere where electric and magnetic observations have confirmed the mode of propagation for many of the various emissions. For a complete discussion of the instrumentation, see Scarf and Gurnett (1977).

2. UPSTREAM WAVES AND BOW SHOCK TURBULENCE

Besides radio emissions, which can often be observed great distances from a planetary magnetosphere, upstream plasma waves are among the first indicators to an approaching spacecraft of the existence of the interaction of the solar wind with the magnetosphere. In the outer heliosphere, the solar wind plasma is tenuous and the magnetic field is very weak, on the order of 0.1 nT (Ness et al., 1986), and the sonic and Alfvenic Mach numbers are very large (Bagenal et al., 1987). Also in the distant heliosphere the Parker spiral angle is very close to 90°, hence, a spacecraft approaching the nose of a magnetosphere as Voyager 2 did at Uranus will likely observe a high Mach number, thin, quasi-perpendicular shock. In this configuration of trajectory and magnetic field orientation, it is not likely that the spacecraft will be magnetically connected to the magnetosphere or its bow shock for a very long distance upstream. Nevertheless, Voyager 2 did observe extensive upstream wave activity in addition to the bow shock itself (Gurnett et al., 1986). Observations of energetic particles were also observed in the upstream region by the Low Energy Charged Particle (LECP) investigation on Voyager 2 (Krimigis et al., 1986; Mauk et al., 1987; Krimigis et al., 1988; Cheng et al., this volume). As we shall see, the energetic particles are likely associated with the observed upstream waves.

2.1 Observations of Upstream Langmuir Waves

As can be seen in Figure 2, there is an extensive region upstream of the bow shock where waves of up to 100 μV/m are observed over an interval of more than a day when Voyager 2 was up to 80 R_U from Uranus. The waves are seen predominantly in the 1.78- and 3.11-kHz channels; based on solar wind plasma observations (Bridge et al., 1986, Bagenal et al., 1987) 2 to 3 kHz would be very close to the electron plasma frequency f_p where f_p [Hz] = $8980\sqrt{n_e}$ with n_e being the local electron density in cm^{-3} and f_p is in units of Hertz. The bursty nature of the waves is quite apparent in Figure 2, even though the plotted values represent 144-second averages. Structure is seen in these emissions at the 4-second resolution of the spectrum analyzer.

The upstream wave activity observed in Figure 2 indicates that Voyager 2 was magnetically connected to the Uranian bow shock for significant periods of time prior to crossing the bow shock, since the waves near f_p are driven by electrons which have been accelerated at the shock and stream into the upstream solar wind. Given the nominal Parker spiral magnetic field configuration, which is almost purely azimuthal at Uranus, Voyager could only detect the waves if extraordinary field direction changes occurred, that is, a configuration with a large radial component, or if the spacecraft were very close to the bow shock. In fact, it is likely both conditions occurred. For the extended interval of upstream activity on January 23, there is evidence of a substantial radial component of the field, (Krimigis et al., 1988) providing the condition of magnetic connection

to the shock, even if the shock were a considerable distance away, as was likely the case at the time.

On the other hand, the upstream activity observed prior to the shock encounter on January 24 was primarily due to the very close proximity of the spacecraft to the shock, making the field orientation less important. What is remarkable about the upstream waves on January 24 is that they occurred over such an extended interval, about 4 hours. During the 4-hour interval Voyager was generally connected with the shock (Krimigis et al., 1988); and the close proximity of the boundary during this time relaxes, considerably, the geometrical constraints on the magnetic field. During both intervals of upstream wave activity Krimigis et al. (1988) reported enhancements of protons with $28 < E < 137$ keV coming from the direction of Uranus, but no evidence of electrons. While we expect electrons to be responsible for the Langmuir waves, it is possible that these fell below the 28 keV lower limit of the LECP and above the 6 keV limit of PLS as was the case at Jupiter (Gurnett et al., 1981). Another possibility for the generation of the Langmuir waves is the ion beams, themselves. Given a solar wind temperature of about 3 eV (Bagenal et al., 1987), the 28-keV ions observed would appear as a very cold beam; such a distribution could excite ion Buneman modes, in particular the electron plasma oscillation branch.

Waves near f_p in the region upstream of planetary bow shocks are quite common and have been studied extensively at the Earth and Jupiter (Scarf et al., 1971; Gurnett and Frank, 1975; Filbert and Kellogg, 1979; Gurnett et al., 1981). These waves are often called electron plasma oscillations or Langmuir waves. They are typically

quite intense, among the most intense waves observed in the vicinity of a planetary magnetosphere and are often quite narrowbanded.

No detailed spectra of the Uranian Langmuir waves were obtained because of the limited number of wideband frames affordable at the distance of Uranus owing to the large amounts of data required for the high temporal and spectral resolution data. From terrestrial and Jovian studies we know, however, that the waves are quite narrowbanded and bursty. From terrestrial observations with spacecraft having wave magnetic field sensors we also know that these emissions are electrostatic in nature; there is no detectable magnetic component to the waves. By analogy, we assume the same is true of the Uranian examples. The fact that the emissions sometimes appear in two of the Voyager channels in Figure 2 does not necessarily mean the Uranian emissions have a broad spectrum; it is more likely the emissions lie somewhere between the center frequencies of adjacent channels and the filter skirt response to the off-center frequencies is sufficient to account for the intensities in both channels.

At Jupiter, Gurnett et al. (1981) discussed the detailed spectral and temporal behavior of the Langmuir waves. There, very short bursts of waves occurred at frequencies just above and below the primary line at f_p. Gurnett et al. suggested that the bursts were of an intensity that was close to exceeding the criterion for the creation of solitons, wherein the electric field increases and plasma is forced outward due to the ponderomotive force. This process proceeds very rapidly until the solitons collapse. Nicholson et al. (1978) provide a thorough review of soliton theory. However, it is likely that heat

flows are strong enough to explain the waves at frequencies well separated from f_p without resorting to the nonlinear theory.

The dispersion relation for Langmuir waves assuming weak turbulence is

$$f^2 = f_p^2(1 + 3k^2\lambda_D^2) \qquad (1)$$

where k is the wave number and λ_D is the Debye length. The growth of the Langmuir waves is one of the classical problems in plasma physics in that it involves a very simple distribution function, a double-humped velocity distribution. Nevertheless, we still do not have a satisfactory understanding of the generation mechanism. The basic idea is clear, however. The bow shock serves as a place where electrons can be accelerated and directed back upstream into the solar wind. This beam of electrons forms a double hump in the electron distribution function when added to the ambient solar wind electron distribution. It is easily shown that such a distribution is a source of free energy and is unstable to Langmuir waves. The theory still does not explain the nonlinear beam stabilization processes that keep the Langmuir waves from completely disrupting the beam (Papadopoulos et al., 1974). It is also possible for waves near f_p to be driven by a strong electron heat flux in the solar wind as observed at Jupiter (Moses et al., 1984), or by the observed high energy ion beams as suggested above.

Other waves common in the upstream region at Earth and Jupiter include ion-acoustic waves, which, after being Doppler shifted by the solar wind flow, can occur at frequencies up to $f_{max} = v_{sw}/2\pi\lambda_D$ where v_{sw} is the solar wind velocity. There is little or no evidence of

these emissions in the Uranus data set, however. The 48-second waveform samples obtained once or twice per day provide the best opportunity to observe such sporadic emissions, but there is no evidence for ion-acoustic waves in those samples. Besides the low duty cycle for the waveform data, relatively intense low frequency interference covering a broad frequency range centered on about 200 Hz would make it very difficult to discern such emissions were they present. There are numerous low frequency bursts, some of which can be seen in Figure 2, which appear in the spectrum analyzer data set. It is quite likely that some of these bursts correspond to ion acoustic waves, however, the spacecraft attitude control system interferes with the plasma wave instrument at frequencies below about 1 kHz, so it is not possible to say for certain that any of the randomly occurring bursts are due to real plasma wave signals. Ion-acoustic waves are not restricted to occurring near planetary bow shocks; Kurth et al. (1979c) showed evidence of these emissions in the solar wind well separated from any bow shock or interplanetary shocks. Ion-acoustic waves also occur in the vicinity of interplanetary shocks.

2.2 Bow Shock Turbulence

Voyager crossed the bow shock once on the inbound leg of the trajectory and that shock has been studied in detail by Bagenal et al., (1987). The plasma wave instrument detected broadband electric field enhancements shortly after 0730 SCET (spacecraft event time) which resemble the type of spectrum observed at the other planetary bow shocks (Gurnett et al., 1986), however, the wave signature was

unusually irregular and diffuse (Scarf et al., 1987). The spectrum was consistent with the lower characteristic frequencies of the solar wind plasma due to the very low plasma density (0.05 cm^{-3}) and weak magnetic field (0.19 nT) in the solar wind in the vicinity of Uranus at the time of the Voyager encounter (Bagenal et al., 1987).

On the outbound leg, the spacecraft encountered the bow shock numerous times as recorded by the Voyager magnetometer and plasma instruments (Ness et al., 1986; Bridge et al., 1986). While some of the shock crossings listed by these two initial reports agree rather well, the two lists contain substantial differences. Nevertheless, the plasma wave investigation also observed signatures associated with some of the reported crossings (Gurnett et al., 1986); there were some, however, where no clear signature was seen in the wave data. At this point in time it is not clear whether some of the shocks simply do not show a wave signature (this would be an exceptional result) or that the initial lists contain questionable identifications as evidenced by the lack of agreement cited above. All shocks reported by both the magnetometer and plasma investigations show a clear plasma wave signature. One possible explanation for the shocks which show little or no wave signature is that the turbulence is so sporadic and impulsive that the 4-second spectrum analyzer sweep is too slow to catch the increases (Scarf et al., 1981).

As reported by Bagenal et al. (1987), the conditions for the inbound shock crossing were ideal for a quasi-perpendicular shock, where the normal to the shock surface was nearly perpendicular to the impinging solar wind magnetic field. In contrast, the outbound crossings occurred on the dawn-side flank of the magnetotail and the

nominal field orientation leads to a quasi-parallel shock configuration. Striking differences are seen in the spectrum of plasma wave turbulence seen in the inbound versus outbound shocks (see, for example, Figure 2 of Scarf et al., 1987). Figure 3 shows 1-minute average and peak spectra for the inbound shock as well as a shock observed near 2300 SCET on January 27 1986 on the outbound leg. The high frequency portion of the two spectra are similar, with waves extending up to a few kHz, consistent with the solar wind plasma frequency. At frequencies between about 30 and 100 Hz, however, the outbound shock shows almost no wave activity at all. There is evidence of shock-associated emissions in the 10-Hz channel, however. The other outbound shocks exhibiting some wave signature tend to follow the trend of the shock displayed in the right-hand panel of Figure 3. Whether the difference in the inbound and outbound spectra is due to the quasi-perpendicular/quasi-parallel differences, or to some other factor is not known at this time.

The modes responsible for the spectra in Figure 3 have not been identified with any degree of certainty at this time and we have only the electric field spectrum to use for clues since Voyager has no wave magnetic field sensor, polarization measurements for plasma waves, and there are no wideband data available within the shock. We can draw on work at other planets, however, for some clues, assuming conditions are not drastically different at Uranus compared to Jupiter or Saturn. One possibility for the higher frequency component, that centered near 0.5 kHz in Figure 3, is a Buneman mode (Moses et al., 1988). These intermediate frequency waves in the inbound spectrum could also be

ion-acoustic-like modes (Scarf et al., 1979; Scarf et al., 1981). As pointed out by Melrose (1980), the Buneman instability transforms to the ion-acoustic instability in a manner very similar to the way the two-stream instability makes the transition to the bump-on-tail. The wave spectrum bandwidth broadens as one moves from a cold to warm plasma regime. The lower frequency component in the outbound spectrum in Figure 3, near 10 Hz, is likely to be a whistler mode, based on a magnetic field strength of about 0.5 nT (Ness et al., 1986). This field strength gives an electron cyclotron frequency of about 14 Hz.

The wave turbulence in shocks has been related to particle acceleration, at least in the Earth's bow shock (see Tsurutani and Rodriguez, 1981 and references therein; Lee, 1982). There has also been much speculation that the wave turbulence in a collisionless shock is responsible for heating the plasma, however, recent studies (Goodrich and Scudder, 1984; Scudder et al., 1986a,b; Mellott, 1986) suggest the plasma waves in the terrestrial bow shock are not required to produce the amount of heating observed; the potential drop across the shock is sufficient, at least in the reported cases (Scudder et al., 1986a). Moses et al. (1985, 1988) find, however, that waves in the shock foot at Jupiter and Saturn are responsible for the observed electron heating through electrostatic waves generated by reflected ions. Detailed analyses of the Uranian shocks have only been initiated recently; preliminary calculations indicate that the wave amplitudes are too weak (at least at the inbound shock) to explain the heating because of the high ion temperatures of ~4 eV (Bagenal et al., 1987) which restricts the ion-beam instability (S. Moses, private communication, 1988).

3. BERNSTEIN EMISSIONS

Bernstein emissions, also commonly referred to as $(n + 1/2)f_c$ emissions are very common in planetary magnetospheres including the Earth, Jupiter, and Saturn (Kennel et al., 1970; Kurth et al., 1980a; Kurth et al., 1983). The preferred location for these emissions in the terrestrial magnetosphere is beyond the plasmapause at the magnetic equator (Christiansen et al., 1978). At Jupiter the bands are very tightly confined to magnetic latitudes of one or two degrees and observed almost exclusively inside of about 23 R_J. Saturn's Bernstein waves are also located in the inner magnetosphere, but show a weaker magnetic latitude confinement than at Jupiter.

The Bernstein emissions are electrostatic waves that are driven by a variety of free energy sources with a positive slope with respect to the velocity perpendicular to the magnetic field in the electron distribution function and can be quite intense, up to several mV/m at the Earth. For many years, the Bernstein waves were thought to be the primary source of pitch-angle scattering of terrestrial plasma sheet electrons forming the diffuse aurora (Lyons 1974) although Belmont et al. (1983) have cast some doubt on this conclusion based on an extensive survey of $(n + 1/2)$ band intensities in the terrestrial magnetosphere.

It was not surprising to find the familiar Bernstein waves in the Uranian magnetosphere (Gurnett et al., 1986). Kurth et al. (1987) reported the emissions as a prominent part of the plasma wave spectrum

at Uranus, second only to the whistler mode hiss and chorus observed in the inner Uranian magnetosphere discussed below. In this section we will review some of the general characteristics of the Bernstein emissions and those at Uranus, in particular.

3.1 Observations of Bernstein Waves at Uranus

Figure 4 summarizes the locations, frequencies, and intensities of the Bernstein waves observed in the Uranian magnetosphere (Kurth et al., 1987). One of the first indications of the effect of the extreme tilt of the magnetic dipole at Uranus was the occurrence of the most prominent example of Bernstein emissions not in the inner magnetosphere near the ring-plane crossing, but at the magnetic equator far out on the dayside of the magnetosphere at about 11.5 R_U. In Figure 4 this event can be seen centered at about 1315 SCET on January 24 primarily in the 1- and 1.78-kHz channels. Other examples are visible in Figure 4 closer in toward Uranus, but the Voyager trajectory did not take the spacecraft through the magnetic equator again while the spacecraft was closer to Uranus.

A detail of the event near 1300 SCET is shown in Figure 5. In this expanded view of the plasma wave spectrum from 311 Hz through 3.11 kHz, it is clear the Bernstein waves are bursty, showing order-of-magnitude intensity variations on times scales of a few seconds, and cover a fairly broad range in frequencies. The burstiness of these emissions is evidence that the waves are electrostatic, but recall that a true determination of the electrostatic character of the waves is not possible with the Voyager sensor. The amplitudes of these emissions are in the range of 100 μV/m.

A few words are in order about the spectral character of the Bernstein emissions. Based on numerous observations in the terrestrial magnetosphere (Kennel et al., 1970; Scarf et al., 1973) it is clear the emissions are composed of one or more narrow bands lying between harmonics of the electron cyclotron frequency. The $(n + 1/2)f_c$ nomenclature stems from the spacing between the bands of about f_c and the fact the bands are between the actual harmonics of f_c, even though they very often do not lie exactly half-way in between.

Hubbard and Birmingham (1978) classified several types of occurrences of the $(n + 1/2)$ bands. Generally speaking, the bands appear in families. Often, the bands start just above f_c and appear between each harmonic between f_c and f_p, with the lowest bands having the highest intensity. Sometimes, the harmonic band including the upper hybrid resonance frequency $f_{uhr} = \sqrt{f_p^2 + f_c^2}$ contains a band and this one can often be the most intense (Kurth et al., 1979b). When the upper hybrid band is observed, it may be that the lower harmonics are not observable at all. There are other cases where the lowest $(3f_c/2)$ harmonic is observed alone, as well.

Returning to Figure 5, now, it is clear that the Voyager spectrum analyzer is not sufficient to resolve the different harmonic components; the higher resolution wideband measurements would have been quite useful here, however, the data rate requirements precluded the transmission of enough of these high resolution observations to cover this event. It is clear from the location of the emissions on a frequency scale set by the baseline of the various channel outputs and the superimposed cyclotron harmonics that emissions in several of the bands are present. When the finite filter bandwidths of the spectrum

analyzer are taken into account, the actual number of harmonics present is indeterminable, but Kurth et al. (1987) suggest the strongest band, corresponding to the band including f_{uhr}, is between 3 and $4f_c$. The upper hybrid band, then, is near $7f_c/2$.

The other evidence for Bernstein emissions at Uranus can be found in Figure 4 by looking for bursty emissions in the channels at or above the electron cyclotron frequency profile given by the solid line. Generally, the remaining emissions are rather weak, averaging about 30 μV/m and are scattered primarily near closest approach and on the outbound leg. It is not surprising that the emissions close in are weak compared to the event in Figure 5 because of the less favorable conditions for growth off the magnetic equator. The conditions for growth of these waves require not only large temporal growth rates, but also sufficiently long path lengths through the region of growth in order to attain reasonable amplitudes. Various studies (c.f. Engle and Kennel, 1984) have shown that the Bernstein waves tend to be trapped at low magnetic latitudes and propagate primarily in azimuth about the planet. Given a region of positive growth, the magnetic equator can be an excellent location to support the growth of waves to large amplitudes. Had Voyager traversed the magnetic equator closer to Uranus than in the Figure 5 event, it is likely even more intense waves would have been observed.

3.2 Theory of the Bernstein Emissions

We do not propose to provide an in-depth discussion of the theory behind the Bernstein emissions here, but it is important to discuss some of the important aspects of the generation of the waves. A

number of detailed theoretical treatments of the emissions are in the literature (see Ashour-Abdalla and Kennel, 1978a and references therein). The dispersion relation governing the emissions is the Harris (1959) dispersion relation. The key for growth of the waves is to have a region in the electron velocity distribution f(v) for which $\partial f/\partial v_\perp$ is positive. The first distribution function used which provided growth was a ring distribution with a delta function (Fredricks, 1971). This distribution is quite severe and unrealistic so Young et al. (1973) showed that the addition of cold electrons greatly reduced the requirements on the electron distribution function which would support wave growth. Soon, the canonical distribution used to model the (n + 1/2) emissions was one in which there was a loss cone feature in the hot electrons with core of cold electrons. Ashour-Abdalla and Kennel (1978a, b) and Hubbard and Birmingham (1978) showed that varying the ratio of hot to cold electrons and their temperatures one could generate growth in various harmonics or ranges of harmonics, similar to those observed.

Shortly thereafter Rönnmark et al. (1978) and Kurth et al. (1979a) did comparisons between observed $(n + 1/2)f_c$ spectra and theoretical growth rate calculations to show qualitative agreement between the theory and observations. Kurth et al., (1980b) went further and showed that the actual form of the distribution is not all that critical; not only do loss cone features provide the free energy for the emissions, but other distributions with a positive $\partial f/\partial v_\perp$ feature such as a hot shell would serve as well.

Perhaps it is this relative insensitivity to the actual form of the distribution function which enables the ubiquitous occurrence of

these electrostatic waves in planetary magnetospheres, in spite of dramatic differences in plasma and energy sources in the various magnetospheres.

Barbosa and Kurth (1980) derived an expression for the critical flux of anisotropic electrons ($E_{perp} > E_{par}$) required to amplify the $3f_c/2$ band by 10 e-foldings. Kurth et al. (1987) modified the expression for Uranus to the following form:

$$Tj^*_\perp = 5.4 \times 10^4 \left(\frac{T/T_c}{4}\right)^2 \left(\frac{T_c}{30\ eV}\right) cm^{-2}s^{-1}sr^{-1} \qquad (2)$$

where they have used 0.23 G as the surface field of Uranus, R_U = 25,600 km, $n_e = 3.9 \times 10^{-2}$ cm^{-3}, R = 11.5, $\delta\bar{\omega} = 0.1$, and $\bar{\omega} = 1.5$ in the formulation by Barbosa and Kurth (1980); T is the electron temperature and T_c is the temperature of the cold, background electrons. Kurth et al. (1987) used a value of 10-30 eV for the background electron temperature, based on that being a typical temperature measured by PLS (Bridge et al. 1986; McNutt et al., 1987) closer to the planet. The above expression for the critical flux evaluated at the magnetic equator crossing by Voyager 2 (see Figure 5) is 3×10^5 $cm^{-2}s^{-1}$ assuming an effective solid angle of about 2π compared to a measured flux of about the same value (Bridge et al. 1986).

This good agreement with the theory is somewhat compromised by the subsequent report of Sittler et al. (1987) that the electrons measured by PLS in the vicinity of the magnetic equator crossing are very close to threshold and there is no solid evidence for electrons below about

1 keV at this location unless they are as cold as 1 eV. However, the electron density derived from the existence of the Bernstein emissions by Kurth et al. (1987) (see below) is almost an order of magnitude greater than that reported by Sittler et al. (1987) for the same time period. The tentative conclusion can only be that there are significant fluxes of electrons either near 1 eV or higher than the 6 keV limit of the PLS to account for the density. The resonant energy of electrons reported by Kurth et al. (1987) of a few hundred eV may hold in the inner magnetosphere, but the lack of observed plasma fluxes at 11.5 R_U (Sittler et al., 1987) makes it difficult to confirm the resonant energy for the equatorial event.

Lyons (1974) recognized the ability of strong electron cyclotron emissions to pitch-angle scatter electrons of a few keV and, hence, represent a viable means of precipitating electrons into the diffuse aurora. While Belmont et al. (1983) have discounted Lyons' conclusion that these electrostatic waves could, alone, account for the diffuse aurora at Earth, largely due to more accurate, lower intensities for the waves than those reported earlier, the ability of the waves to pitch angle scatter electrons remains. Hence, the Bernstein waves at Uranus must be viewed as a scattering mechanism. The low amplitudes reported herein are quite possibly misleading since it is likely that more intense emissions lie near the magnetic equator in the inner magnetosphere not sampled by Voyager. Unfortunately, we cannot assess the importance of the scattering due to these waves with the incomplete survey provided by the Voyager 2 trajectory.

3.3 Density Profile Based on Bernstein Emissions

Since the frequency range over which the $(n + 1/2)f_c$ emissions can be observed is generally between f_c and f_{uhr}, an analysis of the occurrence of these electrostatic emissions can provide some independent information on the electron density. Kurth et al. (1987) made use of this technique to derive a partial plasma density profile for the Uranian magnetosphere; the results of that study are shown in Figure 4 by the dashed line.

While Kurth et al. (1987) provide a detailed description of how this profile was derived, the key to the process is based on knowing that the upper frequency limit for the Bernstein bands is approximately the upper hybrid resonance frequency, which yields the plasma frequency, hence, density because the cyclotron frequency is well known. For example, at the magnetic equator crossing the highest frequency band, which is also the most intense, is likely to be the upper hybrid band. Kurth et al. deduced a plasma frequency of 1.6 kHz, or a plasma density of about 0.03 cm^{-3} for the center of this event at 1315 SCET on January 24. In fact, it is not certain that this is the plasma density because it is possible that only the lower harmonic $(n + 1/2)$ bands are being observed, in which case 0.03 cm^{-3} is a lower limit to the density at this time.

In the region after closest approach the transition from the bursty emissions above f_c to the smooth radio emissions at higher frequencies provides another set of information on the density. Here it was necessary to assume a propagation mode for the radio emissions to know if the cutoff of the radio waves was the left-hand, ordinary

(L-O) or right-hand, extraordinary (R-X) cutoff (or whether the cutoff frequency was the plasma frequency or f_R, the right-hand cutoff) (Stix, 1962) where

$$f_R = \frac{f_c}{2} + \left(f_p^2 + \frac{f_c^2}{4}\right)^{1/2} \qquad (3)$$

Kurth et al. assumed the radio waves are propagating in the R-X mode in order to come up with the profile shown in Figure 4. This choice provided a great deal of consistency with the PLS observations of the density during the post-closest approach interval and has been confirmed by recent radio astronomy studies (Kaiser et al., 1988).

The dashed-line profile in Figure 4 is based primarily on the dots located at various points on the profile. At those times, some specific piece of information was available in order to come up with an estimate of the density. The dashed line between these dots is a simple smooth curve and, as such, may or may not be accurate.

4. WHISTLER MODE EMISSIONS

As mentioned in the Introduction, the dominant plasma wave phenomenon in the Uranian magnetosphere is the band of whistler mode emissions below f_c in the inner Uranian magnetosphere (Gurnett et al., 1986). In this section we will describe the emissions, discuss the implications for pitch-angle scattering implied by the observed intensities, and place the inferred precipitating fluxes into perspective with independent measurements of the diffusion coefficient.

4.1 Observations of Whistler Mode Waves

Figure 6 summarizes the plasma wave spectrum for the inner magnetosphere of Uranus. The spectrum analyzer data shown here covers the radial distance range inward of about 8 R_U and is dominated by the intense band of emissions consistently below the f_c contour based on the OTD model field strength given by Ness et al. (1986). The other signals present below the cyclotron frequency include the sharply peaked emission at the ring plane crossing due to the effect of micron-sized dust particles impacting on the spacecraft at about 1715 SCET (Gurnett et al., 1987) and a band of signals below the whistler mode at 56 and 100 Hz between about 1930 and 2030 SCET tentatively identified as lower hybrid resonance emissions by Coroniti et al. (1987).

The whistler band in Figure 6 extends from as high as about 0.5 to 0.2 f_c down to less than about 0.1 f_c. The band is observable over almost the entire interval plotted except for several minutes around

1930 when numerous bursty emissions are observed but the whistler mode band is clearly missing. An obvious inbound-outbound asymmetry is also apparent with the outbound interval beginning around 1950 SCET to about 2100 SCET being the most intense. In fact, Scarf et al. (1987) label these as the most intense whistler mode emissions observed in the outer planets' magnetospheres.

Across the top of Figure 6 are marked six times labeled by the letters A - F. These markers refer to brief high spectral and temporal resolution snapshots of the frequency-time spectrum obtained with the Voyager wideband receiver. These snapshots are shown in Figure 7 (Gurnett et al., 1986). The six panels in Figure 7 show the detailed frequency-time variations of the emissions which the whistler mode band comprises. The most striking effect is the variation in bandwidth as f_c rises and falls. (Keep in mind the spectrograms in Figure 7 have a linear frequency scale versus the logarithmic frequency scale in Figure 6.)

Panels A, C, E, and F all show the presence of a more-or-less featureless band of what we call hiss, although audio recordings, particularly of frames E and F reveal a considerable amount of structure not readily apparent in the spectrograms. Grabbe (1988a,b) has attempted to explain some of this structure as a propagation effect of whistler waves on the resonance cone passing through density and/or magnetic field inhomogenieties. Frame B shows the presence of discrete rising tones growing out of the hiss band at lower frequencies. These tones are easily recognized as typical chorus elements, strikingly similar to those observed at Earth (Helliwell,

1965) and Jupiter (Coroniti et al., 1984). The panel labeled D is taken from the above-mentioned whistler band gap and consists of very bursty, probably electrostatic emissions (Kurth et al., 1986). An identification of these modes would lead to some very interesting clues as to the source of the whistler band gap, but is beyond the scope of this review.

Figure 8 shows a detailed amplitude versus frequency slice through Panel F in Figure 7, averaged over 0.6 seconds. It is clear from this illustration that the band of intense emission extends over a frequency range from 0.15 to 0.27 f_c as referenced to the local magnetic field. The normalized frequency scale $\bar{\omega}$ at the bottom of Figure 8 is the frequency divided by the equatorial value of the cyclotron frequency f_{ce} measured on the same field line using the OTD magnetic field model (Ness et al., 1986).

4.2 Whistler Theory

Coroniti et al. (1987) have analyzed the effect of the intense whistler mode hiss on energetic electrons. The result is of fundamental importance to understanding the physics of the Uranian magnetosphere and, specifically, the Uranian aurora, and we summarize the line of reasoning followed by Coroniti et al., here.

The basis for the theory is the classical work by Kennel and Petschek (1966). The whistlers resonate with energetic electrons; an anisotropy in the resonant part of the electron distribution function provides the free energy source for the waves and the resulting effect on the electrons is pitch-angle diffusion. The minimum energy for cyclotron resonance with a parallel propagating whistler is

$$R = \frac{B^2}{8\pi n_e} \left(\frac{1 - \bar{\omega}}{\bar{\omega}}\right)^3 \qquad (4)$$

The course taken by Coroniti et al. (1987) was to build a model for the plasma based on observations of the electrons, launch whistlers from the magnetic equator and ray trace to the spacecraft while calculating gain along the path, match two anisotropy parameters in the model to obtain the best fit of the gain to the measured spectrum, and calculate a bounce-averaged diffusion coefficient. Given the diffusion coefficient, they went on to calculate scattering lifetimes and compared those to minimum precipitation lifetimes to find the range of energies over which electrons were on strong diffusion. Given the strong diffusion limit, then, precipitation fluxes, hence, precipitating energy could be calculated and compared with the 10^{11} W Broadfoot et al., (1986) required as precipitation of 10 keV electrons to drive the observed UV aurora.

Coroniti et al. (1987) restricted their study to the time interval between 2000 and 2100 SCET when the whistler mode intensities were at their peak. In fact, they limited their study to two times, 2011 and 2035 SCET; the former time was when the emissions peaked in the 562-Hz channel of the spectrum analyzer and the 2035 time period was chosen because of the high resolution wideband data available then (see panel F of Figure 7 and Figure 8).

The first step in the calculation was to develop a credible model of the plasma from the location of the spacecraft to the magnetic equator in this region of the magnetosphere. As is clear in Equation 4, the plasma density is an important factor in determining the

resonant particle energies. The density profile of Kurth et al. (1987) was used as a basis for this, but supporting evidence from the PLS instrument (McNutt et al., 1987) as well as independent considerations on the basis of the whistler mode signals, themselves, were used. Coroniti et al. used the following formulation for density as a function of L:

$$n_e = 2.2(4.8/L)^{1.44}\ cm^{-3}. \qquad (5)$$

The density was assumed to be constant along an L-shell to the magnetic equator, a reasonable model since the spacecraft was only about 15° above that plane during this interval and there are no significant populations of heavy ions to cause mass loading and related effects.

The whistler mode emissions imply the existence of large fluxes of energetic electrons with an anisotropy which can drive the emissions. Figure 9 shows the fluxes of 22 - 183 keV electrons as observed by the LECP instrument on the same time scale as the spectrum analyzer data and it is clear that intense fluxes of energetic electrons are present at the same time as the intense whistler mode waves. Unfortunately, the energy range from the 6-keV upper limit of the PLS instrument to the 22 keV lower limit of the LECP instrument is a crucial gap to be included in these considerations and a model for the electrons in this gap was formulated. An anisotropic Maxwellian was assumed for the warm electrons in the gap, matching both the differential flux and the derivative of the differential flux at the 27.5 keV center energy of the lowest energy LECP electron channel. The model is shown by the

dashed line in Figure 10. As a check, the integral flux was compared to that reported by Bridge et al. (1986) and the values matched to within a factor of two.

To explain the relative gain at different frequencies requires that the anisotropy of the warm electrons is different from that of the hot electrons. Since only the anisotropy for the hot electrons is available, a model was assumed which gave a smooth variation in anisotropy over energy with a match at the 27.5 keV center energy of the lowest LECP channel. Hence,

$$A_w(t) = [A_w(0) - A_E](1 - t^2/t_E^2)^2 + A_E \qquad (6)$$

where A_E is the pitch angle anisotropy (measured), $A_w(t)$ is the anisotropy of the warm electrons as a function of energy, t is energy, and t_E is 27.5 keV. The match condition requires that $A_w(t_E) = A_E$.

The plasma model is complete, then, and is entirely specified by two anisotropies, $A_w(0)$ and A_E. Obviously, the magnetic field model is also important to the problem, but that is available in the form of the OTD model (Ness et al., 1986).

The next step in the calculation is to launch the waves from the magnetic equator and calculate the path-integrated gain as a function of frequency. The ray tracing of Coroniti et al. (1987) was accomplished by taking into account the rotation of the whistler mode wave normal angle due to the curvature in the field and the gradients in the wave index of refraction following Kimura (1966), Thorne and Kennel (1976), Burtis and Helliwell (1976), and Church (1982). Because of the limited range of latitude required (0 to 16.5°) a

simple finite differencing scheme was used to do the integration. The gain calculation retained only the first order cyclotron resonance and the Landau damping contributions, since these are generally the strongest.

In finding the gain at a given frequency, a variety of initial wave normal angles was used in order to find the maximum growth. The two anisotropies, $A_w(0)$ and A_E were adjusted iteratively to give the maximum gain as a function of frequency which best matched the observed spectrum. The result of this approach is given in Figure 11, where the solid dots are the calculated gains and the X's are the measured power spectrum. The two sets of points were normalized by equating the observed and calculated peak power spectral densities. The anisotropies which provided these fits are $A_E = 0.53$ (0.56) and $A_w(0) = 0.43$ (1.1) at 2011 (2035) SCET. A variance analysis was performed which showed that independent variations of 0.1 in the anisotropies seriously degraded the fits.

Differences in the warm electron model and the effects of launching the waves at locations other than the equator are considered to be minor perturbations to the calculation; the actual calculation simply shows the consistency between the observations and the amplification model.

The non-relativistic diffusion coefficient for parallel whistlers can be written as

$$D_{\alpha\alpha} = 4.4 \times 10^{4} n^2 E^2(f) \left| \frac{v_g}{v_g + |v_\parallel|} \right|_{\omega = \omega_r} \qquad (7)$$

where n is the index of refraction and v_g is the group velocity.

Since a whistler will resonate with different energy electrons as it traverses the region of growth, one must calculate a bounce-averaged diffusion coefficient.

The average pitch angle scattering time T_s is roughly the inverse of $D_{\alpha\alpha}$ and the electron fluxes will be at or close to the strong diffusion limit if $T_s < T_{min} = 4L^4R_U/v$, the minimum precipitation lifetime (Kennel, 1969). Coroniti et al. presented the results of the T_s versus T_{min} comparison as in Figure 12. It is readily apparent that the bounce-averaged scattering times are below the minimum precipitation lifetimes for a wide range of electron energies at both times. Electrons in the energy range of about 5 to 40 keV are apparently on strong diffusion for this time interval on L shells of about 6 to 9.

Following Coroniti and Kennel (1970) the precipitating electron flux J_p is related to the trapped flux J_T approximately by

$$\frac{J_p}{J_T} = \frac{T_{min}}{T_L} \qquad (8)$$

where T_L is the electron lifetime which is approximately equal to T_{min}. Hence, the total precipitating energy flux at 2011 SCET is about 1.0 erg/cm^2 (at L = 6.73) and at 2035 SCET (L = 7.64) the precipitating energy flux is about 0.5 erg/cm^2. Since the precipitating flux appears to increase with decreasing L and the intense waves exist over the range of about L = 6 to 9, it is possible the energy flux into the atmosphere exceeds 1.0 erg/cm^2 at L = 6. Broadfoot et al., (1986) reported auroral luminosity near the southern

magnetic pole that would require approximately 10^{11} W from precipitating electrons in the 10-keV energy range. Coroniti et al. (1987), assuming a uniformly illuminated 20° polar cap, estimated this to be about 0.8 erg/cm^2, very close to the calculated precipitating energy fluxes.

As pointed out by Cheng et al. (this volume) as well as Coroniti et al. (1987), the above result leads to some interesting problems. The strong diffusion implies there is a very strong source of a few- to 50-keV electrons. Cheng et al. (1987) find the radial diffusion coefficient to be 10^{-6} - 10^{-7} s^{-1} at L = 7.5, however, for strong diffusion we require $D_{LL}T_{min} > 1$ or D_{LL} to be about 2.5×10^{-4} s^{-1}. One possible explanation would be that there exists strong temporal variations in the fluxes, or a substorm-like injection of 5 - 40-keV electrons. Both Mauk et al. (1987) and Cheng et al. (1987) presented evidence for injections, but Cheng et al. argue against substantial injection events based on the near equality of the inbound and outbound electron phase space densities at L=10.

The precipitation lifetime calculations of Coroniti et al. (1987) are based on the assumptions that all the electric field intensity measured is due to whistler mode waves, that the electric fields are primarily transverse to the Uranian magnetic field, that the index of refraction (based primarily on the electron density) is well known, that the turbulence exists throughout the +/- 16° region, and that the diffusion rate must be maintained along the drift/transport trajectory for at least T_{min}. The first two assumptions are based almost purely on our terrestrial experience. The electron density is consistent

with three independent estimates including McNutt et al. (1987) and Kurth et al. (1987) as well as a self-consistent analysis of the growth rates for the whistler mode waves performed by Coroniti et al. (1987). The good agreement of the ray tracing calculations of the path-integrated gains and the observed waves leave one with confidence that the amplification region must fill the 16° region with little doubt. Finally, the continuously present band of intense whistler mode emissions over the interval from 1950 SCET to 2100 SCET argues strongly that the turbulence is widespread and continuous enough to meet the T_{min} criterion. We must conclude that the precipitation lifetimes are reasonable.

One other conflicting factor one should consider is that the location cited for the strong Uranian radio emissions (c.f. Leblanc et al., 1987; Kaiser et al., 1987; Zarka and Lecacheux, 1987) is generally on much larger L-shells, close to 15 to 20. Given that the radio emissions are driven by an auroral process, it is difficult to reconcile the auroral precipitation on much lower L-shells. On the other hand, Barbosa (1988) suggests the intense radio emission is likely on much lower L-values near L = 4, more consistent with those associated with the strong whistler mode diffusion discussed here.

Coroniti et al. (1987) offer one other possible explanation for the large energetic electron fluxes implied by the whistler mode emissions. The suggestion is that low-energy electrons could experience strong upward energy diffusion prior to being lost to the atmosphere. The idea is based on Kennel (1969), however, significant work is required to fully explore the mechanism.

5. PLASMA WAVES IN THE MAGNETOTAIL

The magnetotail of Uranus is very quiet in terms of the level of plasma wave turbulence there (Gurnett et al., 1986), especially compared with the case at Earth. However, there are waves present in the magnetotail of Uranus and we will review the observations of these waves reported by Kurth et al. (1988) and address the mode of propagation of those waves in this section. Unfortunately, the Voyager observations do not appear to be complete enough to satisfactorily settle upon the wave mode in this case.

5.1 Observations

Figure 13 is an overview of the observations of plasma waves in the magnetotail of Uranus. The plot begins near closest approach and extends to the approximate occurrence of the fourth and partial encounter with the plasma sheet (Ness et al., 1986). While there is a significant data set beyond the end of Figure 13 to the magnetopause, little, if any, plasma wave activity is identifiable in the outer portion of the magnetotail trajectory. The 'D' at the top of Figure 13 locates the abrupt decrease in the fluxes of energetic particles in the Uranian radiation belts (Mauk et al., 1987), hence, the wave events of interest are found later in time than 'D'. In fact, one can identify three regions of wave activity, centered at about 2300 SCET on January 24 and 0300 and 1800 SCET on January 25 1986. These events are confined to extremely low frequencies and in each case appear to be limited on the high frequency side by the contour of f_c

superimposed on the figure based on the magnetic field measurements (Ness et al., 1986).

An additional observation can be made about the three wave events after 'D' in Figure 13. The turbulence occurs before the first neutral sheet crossing (NS1) (Ness et al., 1986), and after the second crossing (NS2). The wave activity is well separated from the magnetic field strength minima associated with the neutral sheet and comparisons with PLS and LECP observations indicate the second and third wave events are not associated with the plasma sheet, either. Further, it is interesting that the activity does not appear between NS1 and NS2, when the spacecraft would be on field lines connected to the dayside, northern magnetic pole.

Figure 14, from Kurth et al. (1988) shows spectra typical of those observed in all three of the tail wave events, although these are only from the second event, near 0200 SCET on January 25. Plotted are 5-minute average spectra and the peak values observed over the same 5-minute interval for two time periods. Both sets of spectra show evidence for a local maximum in the spectrum at about 56 Hz, but the spectrum from 0140 SCET (labeled C) is almost monotone decreasing in frequency. Spectra taken from the third event near 1800 SCET on January 25 do show a simple, monotone decreasing trend with no evidence for a local maximum.

5.2 Interpretation of the Magnetotail Waves

The lack of a magnetic sensor on Voyager sensitive to frequencies up to 100 Hz makes it very difficult to come to any solid conclusions as to the wave mode of the waves observed in the Uranian magnetotail. The fact that the spectrum lies below f_c and the likelihood that $f_p >$

f_c means the wave spectrum is at least consistent with the whistler mode. The other competing interpretation for the waves given by Kurth et al. (1988) is that they are analogous to the broadband electrostatic noise common in the terrestrial magnetosphere. The spectra shown in Figure 14 are reminiscent of those taken at Earth by Gurnett et al. (1976) and Gurnett and Frank (1977).

Further indication that the waves are more like broadband electrostatic noise than whistler emissions comes from an analysis of the locations of the event. Figure 15 shows the location of wave activity against a cartoon model of the plasma sheet taken from Mauk et al. (1987). The last three darkened portions of the Voyager 2 trajectory in this solar-magnetospheric coordinate system correspond to the three wave events from Figure 13. The first of these corresponds very well to the 'horn' of the plasma sheet and the second could be construed as having a relation to the plasma sheet boundary layer. According to this construction, the third event lies deep in the magnetotail lobe, although it is possible for this event to be in the magnetopause boundary layer. Scarf et al. (1984) report broadband electrostatic noise in a similar region at the Earth. The three events, then, occur in regions of the magnetosphere similar to the known locations for broadband electrostatic noise based on terrestrial observations. It is also clear in Figure 15 that the wave activity favors the nightside, southern magnetic field lines, suggesting an asymmetry with the dayside, northern magnetic field lines. Such asymmetries are common in other phenomena observed at Uranus, most notably the Uranian radio emissions almost certainly are primarily

primarily associated with the southern magnetic pole (c.f. Leblanc et al., 1987; Kaiser et al., 1987; Zarka and Lecacheux, 1987).

The broadband electrostatic wave interpretation for the waves suggests that field-aligned ion beams or current instabilities might be responsible for driving the waves (Grabbe and Eastman, 1984; Omidi, 1985; Dusenbery and Lyons, 1985; Ashour-Abdalla and Okuda, 1986, Akimoto and Omidi, 1986). Kurth et al. (1988) looked for evidence of field-aligned ion flows in the LECP data and did find evidence for such distributions, however, the detailed comparison of the LECP flow observations with the occurrence of the wave events was not sufficient to allow a solid correlation to be made.

In summary, it is unfortunate that Voyager 2 did not provide additional information on the nature of the waves observed in the Uranian magnetotail, since a definitive identification of the mode is difficult or impossible without such information. However, it is interesting to observe the presence of the emissions and their location specifically not on or near the neutral sheet. The implication is that the physics of the Uranian magnetotail, as is the case at Earth, is interesting not only in the plasma sheet, but extends through the plasma sheet boundary layer, into the lobe, and to the magnetopause.

6. SUMMARY

In this chapter we have discussed the primary plasma waves observed in the Uranian magnetosphere. It is important to consider that the scope of the chapter is influenced strongly by the preceding work on the Uranian plasma wave observations. There are other emissions that have not been discussed here, such as the unidentified bursty emissions near the outbound Miranda L-shell crossing (Kurth et al., 1986), lower hybrid waves in the vicinity of the more intense whistler mode emissions (Coroniti et al., 1987) as well as others which have not yet been identified. These have been omitted because of our lack of progress on them at this time.

The waves discussed, however, include upstream Langmuir waves and turbulence at the bow shock, Bernstein electrostatic waves, whistler mode chorus and hiss, and low frequency turbulence in the magnetotail tentatively identified as broadband electrostatic noise. Figure 16 is a schematic representation of the magnetosphere adapted from Behannon et al., (1987) and Mauk et al., (1987) with the locations of these major plasma wave types identified. It is important to remember while studying Figure 16 that Voyager 2 sampled only a very small volume of the space represented, hence, considerable liberty has been taken in identifying the various regions.

The upstream Langmuir waves represent the most distant form of wave-particle interactions associated with the magnetosphere of Uranus and are remarkable because of their extensive sphere of influence,

compared with Saturn, for example. In addition to the denoted location in the general solar direction, similar emissions were also observed beyond the dawn flank of the magnetosphere during the outbound portion of the trajectory. The turbulence at the bow shock has many similarities to shock spectra at Jupiter and Saturn, if one takes into account the downward shift of critical frequencies of the solar wind plasma associated with the greater heliocentric distance of Uranus. One characteristic of the outbound bow shock spectra which is remarkable is the notch in the spectrum between the whistler mode turbulence and the ion-acoustic turbulence. While studies of the shocks at Jupiter and Saturn (Moses et al., 1985, 1988) might lead one to expect that the shock turbulence plays an important role in heating electrons, preliminary analyses (S. Moses, private communication, 1988) indicate the wave intensities are too low for significant heating.

The Bernstein waves are pervasive in the inner portion of the magnetosphere. As in the other planetary magnetospheres, these waves have their maximum intensities at the magnetic equatorial plane. The wave amplitudes were modest by terrestrial standards, but because Voyager 2 did not cross the magnetic equator inside of about 11.5 R_U, we can speculate that significantly more intense Bernstein emissions may exist. We know at Earth that these emissions are at least partially responsible for scattering electrons from the plasma sheet into the loss cone to produce the diffuse aurora. Given that significant intensities (~ 1 mV/m) occur for these bands near the equator in the Uranian inner magnetosphere, it is possible that they

could play a role as a loss mechanism to radiation belt, few keV electrons.

The most significant wave activity at Uranus is the whistler mode band which permeates the inner magnetosphere where the electron fluxes are high. In the outbound region on L-shells of 6 - 9 the waves are sufficiently intense to put 5 - 40 keV electrons on strong diffusion and could, therefore, produce the observed UV aurora. Unfortunately, it is not clear how the energetic electrons are resupplied fast enough to support this process in view of the scattering lifetimes of order 10^3 seconds. It is clear, however, that a complete understanding of the processes ongoing in the Uranian magnetosphere cannot be had until the role of these waves is fully reconciled with the other, independent estimates of the diffusion coefficient. Several possibilities for this reconciliation including time variable injections or upward energy diffusion of the electrons prior to precipitation require further consideration.

The final class of waves considered here are those weak, low frequency emissions noted in the horn of the plasma sheet and the magnetotail. While the whistler mode cannot be ruled out for these waves, Kurth et al. (1988) favor a broadband electrostatic noise interpretation for the emissions. Such an interpretation fits in with the terrestrial situation of the electrostatic noise being observed near the plasma sheet and magnetopause boundary layers and on auroral field lines closer to the planet in conjunction with field-aligned ion flows.

In view of the unlikely possibility of returning to Uranus in the near future it is probably folly to discuss goals for additional plasma wave observations there. Nevertheless, several issues raised herein demand attention. The primary one, of course, is to sort out the questions raised by the strong diffusion by whistler mode waves. Certainly an orbiter with a periapsis of 4 R_U or less would be able to sort out the apparent asymmetries in whistler mode intensities and be able to rigorously attribute variations to either temporal or spatial effects. Accompanying energetic electron observations could better characterize substorms or injection effects. Associated observations would have to include high resolution maps of the auroral region and its temporal variations as well as a definitive study of the location of the various radio sources, particularly those associated with the aurora.

Another high priority for a return to Uranus would be to cover the magnetic equatorial region close to the planet in order to better assess the importance of the Bernstein emissions and their potential as a loss mechanism for energetic particles. Even for those emissions measured near 11.5 R_U we have little confidence in the resonant energy of electrons interacting with those waves due to the low electron fluxes measured during that event (Sittler et al., 1987). These emissions are also good candidates for the source of the weak continuum radiation observed by Gurnett et al., (1986) and could also be related to the sporadic narrowband radio emissions near 5 kHz (Kurth et al., 1986).

While many other issues could benefit by a return flight to Uranus a final one which is especially enticing is to understand the dramatic change in the plasma wave spectrum observed by Voyager 2 near 1930 SCET on January 24 as the spacecraft passed through the Miranda L-shell, or alternately, as the spacecraft passed through the convection limit (McNutt et al., 1987; Selesnick and McNutt, 1987). It is within this region that Voyager observed an almost complete drop-out of the otherwise omnipresent whistler band and saw it replaced with very bursty, as yet unidentified emissions. Kurth et al. (1986) also associated this region with the source of the sporadic narrowband radio emissions and the bursty nature of the plasma waves in this region may also relate to the higher frequency bursty radio emissions (Warwick et al., 1986; Evans et al., 1987).

Finally, it should be recognized that a return mission to Uranus will find a dramatically different magnetosphere due to the large variations in sun-magnetic dipole directions over the Uranian year. It would be extremely illuminating, not only from the point of view of wave particle interactions, to observe changes in the magnetosphere over a significant fraction of its orbit around the sun.

ACKNOWLEDGMENTS

The research at the University of Iowa was supported by the National Aeronautics and Space Administration through Contract 957723 with the Jet Propulsion Laboratory. The research at TRW was supported by the National Aeronautics and Space Administration through Contract 957805 through the Jet Propulsion Laboratory.

REFERENCES

Akimoto, K., and Omidi, N. 1986. The generation of broadband electrostatic noise by ion beams in the magnetotail. Geophys. Res. Lett. 13:97-100.

Ashour-Abdalla, M., and Kennel, C. F. 1978a. Nonconvective and convective electron cyclotron harmonic instabilities. J. Geophys. Res. 83:1531-1543.

Ashour-Abdalla, M., and Kennel, C. F. 1978b. Multi-harmonic electron instabilities. Geophys. Res. Lett. 5:711-714.

Ashour-Abdalla, M., and Okuda, H. 1986. Theory and simulations of broadband electrostatic noise in the geomagnetic tail. J. Geophys. Res. 91:6833-6844.

Bagenal, F.; Belcher, J. W.; Sittler, Jr., E. C.; and Lepping, R. P. 1987. The Uranian bow shock: Voyager 2 inbound observations of a high Mach number shock. J. Geophys. Res. 92:8603-8612.

Barbosa, D. D. 1988. Polar cap emission model of Uranian kilometric radiation. Astrophys J. in press.

Barbosa, D. D., and Kurth, W. S. 1980. Superthermal electrons and Bernstein waves in Jupiter's inner magnetosphere. J. Geophys. Res. 85:6729-6742.

Behannon, K. W.; Lepping, R. P.; Sittler, Jr., E. C.; Ness, N. F.; Mauk, B. H.; Krimigis, S. M.; and McNutt, Jr., R. L. 1987. The magnetotail of Uranus. J. Geophys. Res. 92:15,354-15,366.

Belcher, J. W.; Selesnick, R.; McNutt, R.; Sittler, E. C.; and Richardson, J. this volume. The plasma environment of Uranus. Uranus (J. Bergstralh, ed.). Tucson, Arizona: University of Arizona Press.

Belmont, G.; Fontaine, D.; and Canu, P. 1983. Are equatorial electron cyclotron waves responsible for diffuse auroral electron precipitation? J. Geophys. Res. 88:9163-9170.

Bridge, H. S.; Belcher, J. W.; Coppi, B.; Lazarus, A. J.; McNutt, Jr., R. L.; Olbert, S.; Richardson, J. D.; Sands, M. R.; Selesnick, R. S.; Sullivan, J. D.; Hartle, R. E.; Ogilvie, K. W.; Sittler, Jr., E. C.; Bagenal, F.; Wolff, R. S.; Vasyliunas, V. M.; Siscoe, G. L.; Goertz, C. K.; and Eviatar, A. 1986. Plasma observations near Uranus: Initial results from Voyager 2. Science 233:89-93.

Broadfoot, A. L.; Herbert, F.; Holberg, J. B.; Hunten, D. M.; Kumar, S.; Sandel, B. R.; Shewansky, D. E.; Smith, G. R.; Yelle, R. V.; Strobel, D. F.; Moos, H. W.; Donahue, T. M.; Atreya, S. K.; Bertaux, J. L.; Blamont, J. E.; McConnell, J. C.; Dessler, A. J.; Linick, S.; and Springer, R. 1986. Ultraviolet spectrometer observations of Uranus. Science 233:74-79.

Burtis, W. J., and Helliwell, R. A. 1969. Banded chorus: A new type of VLF radiation observed in the magnetosphere by OGO 1 and OGO 3. J. Geophys. Res. 74:3002-3010.

Cheng, A. F.; Krimigis, S. M.; Lanzerotti, L. J.; and Stone, E. C. this volume. Energetic charged particles at Uranus. Uranus, (J. Bergstralh, ed.). Tucson, Arizona: University of Arizona Press.

Cheng, A. F.; Krimigis, S. M.; Mauk, B. H.; Keath, E. P.; Maclennan, C. G.; Lanzerotti, L. J.; Paonessa, M. T.; and Armstrong, T. P. 1987. Energetic ion and electron phase space densities in the magnetosphere of Uranus. J. Geophys. Res. 92:15,315-15,328.

Christiansen, P.; Gough, P.; Martelli, G.; Block, J.-J.; Cornilleau, N.; Etcheto, J.; Gendrin, R.; Jones, D.; Bèghin, C.; and Dècrèau, P. 1978. Geos I: Identification of natural magnetospheric emissions. Nature 272:682-686.

Church, S. R. 1982. The generation and distribution of whistler-mode noise in the Earth's plasmasphere. Ph.D. thesis, Univ. of Calif., Los Angeles, Calif.

Connerney, J. E. P.; Acuña, M. H.; and Ness, N. F. 1987. The magnetic field of Uranus. J. Geophys. Res. 92:15,329-15,336.

Coroniti, F. V., and Kennel, C. F. 1970. Electron precipitation pulsations. J. Geophys. Res. 75:1279-1289.

Coroniti, F. V.; Kurth, W. S.; Scarf, F. L.; Krimigis, S. M.; Kennel, C. F.; and Gurnett, D. A. 1987. Whistler mode emissions in the Uranian radiation belts. J. Geophys. Res. 92:15,234-15,248.

Coroniti, F. V.; Scarf, F. L.; Kennel, C. F.; and Kurth, W. S. 1984. Analysis of chorus emissions at Jupiter. J. Geophys. Res. 89:3801-3820.

Desch, M. D.; Gulkis, S.; Kaiser, M. L.; Leblanc, Y.; Lecacheux, A.; Pedersen, B. M.-; and Evans, D. this volume. Uranus radio emissions. Uranus (J. Bergstralh, ed.). Tucson, Arizona: University of Arizona Press.

Dusenbery, P., and Lyons, L. 1985. The generation of broadband electrostatic noise in the plasma sheet boundary layer. J. Geophys. Res. 90:10,935-10,943.

Engle, J., and Kennel, C. F. 1984. Effect of parallel refraction of magnetospheric upper hybrid waves. Geophys. Res. Lett. 11:865-868.

Evans, D. R.; Romig, J. H.; and Warwick,, J. W. 1987. Bursty radio emissions from Uranus. J. Geophys. Res. 92:15,206-15,210.

Filbert, P. C., and Kellogg, P. J. 1979. Electrostatic noise at the plasma frequency beyond the bow shock. J. Geophys. Res. 84:1369-1381.

Fredricks, R. W. 1971. Plasma instability at $(n + 1/2)f_c$ and its relationship to some satellite observations. J. Geophys. Res. 76:5344-5348.

Goodrich, C. C., and Scudder, J. D. 1984. The adiabatic energy charge of plasma electrons and the frame dependence of the cross-shock potential at collisionless magnetosonic shock waves. J. Geophys. Res. 89:6654-6662.

Grabbe, C. L. 1988a. Extraordinary mode waves on the resonance cone detected on Uranus. Proceedings, Second International Workshop on Radio Emissions from Planetary Magnetospheres. (Graz, Austria, 7-9 September, 1987) in press.

Grabbe, C. L. 1988b. Extraordinary mode resonance cones in the Uranian magnetosphere? J. Geophys. Res. submitted.

Grabbe, C. L., and Eastman, T. E. 1984. Generation of broadband electrostatic noise by ion beam instabilities in the magnetotail. J. Geophys. Res., 89:3865-3872.

Gurnett, D. A., and Frank, L. A. 1975. Electron plasma oscillations associated with type III radio emissions and solar electrons. Solar Phys. 45:477-493.

Gurnett, D. A., and Frank, L. A. 1977. A region of intense plasma wave turbulence on auroral field lines. J. Geophys. Res. 82:1031-1050.

Gurnett, D. A.; Frank, L. A.; and Lepping, R. P. 1976. Plasma waves in the distant magnetotail. J. Geophys. Res. 81:6059-6071.

Gurnett, D. A.; Maggs, J. E.; Gallagher, D. L.; Kurth, W. S.; and Scarf, F. L. 1981. Parametric interaction and spatial collapse of beam-driven Langmuir waves in the solar wind. J. Geophys. Res. 86:8833-8841.

Gurnett, D. A.; Kurth, W. S.; Scarf, F. L.; Burns, J. A.; Cuzzi, J. N.; and Gruen, E. 1987. Micron-sized particle impacts detected near Uranus by the Voyager 2 plasma wave instrument. J. Geophys. Res. 92:14,959-14,968.

Gurnett, D. A.; Kurth, W. S.; Scarf, F. L.; and Poynter, R. L. 1986. First plasma wave observations at Uranus. Science 233:106-109.

Harris, E. G. 1959. Unstable plasma oscillations in a magnetic field. Phys. Rev. Lett. 2:34-36.

Helliwell, R. A. 1965. Whistlers and Related Ionospheric Phenomena. pp. 203-316. Stanford, California: Stanford University Press.

Hill, T. W. 1984. Magnetospheric structures: Uranus and Neptune. Uranus and Neptune (J. T. Bergstralh, ed.) pp. 497-525. NASA Conf. Pub. 2330.

Hubbard, R. F., and Birmingham, T. S. 1978. Electrostatic emissions between electron gyroharmonics in the outer magnetosphere. J. Geophys. Res. 83:4837-4850.

Kaiser, M. L.; Desch, M. D.; Connerney, J. E. P.; and Fung, S. 1988. The source of Uranus' smooth low-frequency radio emissions. Proceedings of the Uranus Colloquium (J. Bergstralh, ed.) (June 28-July 1, 1988) p. 4.13.

Kaiser, M. L.; Desch, M. D.; and Curtis, S. A. 1987. The sources of Uranus' dominant nightside radio emissions. J. Geophys. Res., 92:15,169-15,176.

Kennel, C. F., 1969. Consequences of a magnetospheric plasma. Rev. Geophys. 7:379-419.

Kennel, C. F., and Petschek, H. E. 1966. Limit on stably trapped particle fluxes. J. Geophys. Res. 71:1-28.

Kennel, C. F.; Scarf, F. L.; Fredricks, R. W.; McGehee, J. H.; and Coronith, F. V. 1970. VLF electric field observations in the magnetosphere. J. Geophys. Res. 75:6136-6152.

Kimura, I., 1966. Effects of ions on whistler-mode ray tracing. Radio Sci. 1:269-283.

Krimigis, S. M.; Armstrong, T. P.; Axford, W. I.; Cheng, A. F.; Gloeckler, G.; Hamilton, D. C.; Keath, E. P.; Lanzerotti, L. J.; and Mauk, B. H. 1986. The magnetosphere of Uranus: Hot plasma and radiation environment. Science 233:97-102.

Krimigis, S. M.; Keath, E. P.; Mauk, B. H.; Cheng, A. F.; Lanzerotti, L. S.; Lepping, R. P.; and Ness, N. F. 1988. Observations of energetic ion enhancements and fast neutrals upstream and downstream of Uranus' bow shock by the Voyager 2 spacecraft. Planet. Space Sci. 36:311-328.

Kurth, W. S., 1985. Plasma waves and continuum radiation in planetary magnetospheres. Proceedings, Comparative Study of Magnetospheric Systems (September 9-13) (Pedersen, LeQueau, Roux, and Saint-Marc, eds.) p.497-532. La Londe des Maures, France: Cepadues-Editions.

Kurth, W. S.; Ashour-Abdalla, M.; Frank, L. A.; Kennel, C. F.; Gurnett, D. A.; Sentman, D. D.; and Burek, B. G. 1979a. A comparison of intense electrostatic waves near f_{UHR} with linear instability theory. Geophys. Res. Lett. 6:487-490.

Kurth, W. S.; Barbosa, D. D.; Gurnett, D. A.; and Scarf, F. L. 1980a. Electrostatic waves in the Jovian magnetosphere. Geophys. Res. Lett. 7:57-64.

Kurth, W. S.; Barbosa, D. D.; Gurnett, D. A.; and Scarf, F. L. 1987. Electrostatic waves in the magnetosphere of Uranus. J. Geophys. Res. 92:15,225-15,233.

Kurth, W. S.; Craven, J. D.; Frank, L. A.; and Gurnett, D. A. 1979b. Intense electrostatic waves near the upper hybrid resonance frequency. J. Geophys. Res. 84:4145-4164.

Kurth, W. S.; Gurnett, D. A.; and Scarf, F. L. 1979c. High resolution spectrograms of ion-acoustic waves in the solar wind. J. Geophys. Res. 84:3413-3419.

Kurth, W. S.; Gurnett, D. A.; and Scarf, F. L. 1986. Sporadic narrowband radio emissions from Uranus. J. Geophys. Res. 91:11,958-11,964.

Kurth, W. S.; Gurnett, D. A.; Scarf, F. L.; and Mauk, B. H. 1988. Plasma waves in the magnetotail of Uranus. J. Geophys. Res. submitted.

Kurth, W. S.; Frank, L. A.; Ashour-Abdalla, M.; Gurnett, D. A.; and Burek, B. G. 1980b. Observations of a free-energy source for intense electrostatic waves. Geophys. Res. Lett. 7:293-296.

Kurth, W. S.; Scarf, F. L.; Gurnett, D. A.; and Barbosa, D. D. 1983. A survey of electrostatic waves in Saturn's magnetosphere J. Geophys. Res. 88:8959-8970.

Leblanc, Y.; Aubier, M. G.; Ortega-Molina, A.; and Lecacheux, A. 1987. Overview of the Uranian radio emission: Polarization and constraints on source locations. J. Geophys. Res. 92:15,125-15,138.

Lee, M. A. 1982. Coupled magnetic wave excitation and ion acceleration upstream of the Earth's bow shock. J. Geophys. Res. 87:5063-5080.

Lyons, L. R. 1974. Electron diffusion driven by magnetospheric electrostatic waves. J. Geophys. Res. 79:575-580.

Mauk, B. H.; Krimigis, S. M.; Keath, E. P.; Cheng, A. F.; Armstrong, T. P.; Lanzerotti, L. J.; Gloeckler, G.; and Hamilton D. C., 1987. The hot plasma and radiation environment of the Uranian magnetosphere. J. Geophys. Res. 92:15,283-15,308.

McNutt, Jr., R. L.; Selesnick, R. S.; and Richardson, J. D. 1987. Low-energy plasma observations in the magnetosphere of Uranus J. Geophys. Res. 92:4399-4410.

Mellott, M. M. 1986. Plasma wave signatures of collisionless shocks and the role of plasma wave turbulence in shock formation. Adv. Space Res. 6:25-32.

Melrose, D. B. 1980. Plasma Astrophysics: Nonthermal Processes in Diffuse Magnetized Plasmas vol. 2. New York: Gordon and Breach.

Moses, S. L.; Coroniti, F. V.; Kennel, C. F.; and Scarf, F. L. 1984. Strong electron heat flux modes in Jupiter's foreshock. Geophys. Res. Lett. 9:869-872.

Moses, S. L.; Coroniti, F. V.; Kennel, C. F.; and Scarf, F. L. 1985. Estimation and comparison of quasilinear electron heating in the shock foot at Jupiter and Earth. Geophys. Res. Lett. 12:609-612.

Moses, S. L.; Coroniti, F. V.; Kennel, C. F.; and Scarf, F. L. 1988. Wave-particle interactions in the foot of the Saturnian bow shock. J. Geophys. Res. 93:1785-1793.

Ness, N. F.; Acuña, M. H.; Behannon, K. W.; Burlaga, L. F.; Connerney, J. E. P.; Lepping, R. P.; and Neubauer, F. M. 1986. Magnetic fields at Uranus. Science 233:85-89.

Ness, N. F.; Connerney, J. E. P.; Lepping, R. P.; Schulz, M.; and Voigt, H., this volume. Magnetic field and magnetosphere configurations for Uranus. Uranus (J. Bergstralh, ed.). Tucson, Arizona: University of Arizona Press.

Nicholson, D. R.; Goldman, M. V.; Hoyng, P.; and Weatherall, J. C. 1978. Nonlinear Langmuir waves during type III solar radio bursts. Astrophys. J. 223:605-619.

Omidi, N. 1985. Broadband electrostatic noise produced by ion beams in the Earth's magnetotail. J. Geophys. Res. 90:12,330-12,334.

Papadopoulos, K.; Goldstein, M. L.; and Smith, R. A. 1974. Stabilization of electron streams in type III solar radio bursts. Astrophys. J. 190:175-185.

Ronnmark, K.; Borg, H.; Christiansen, P. J.; Gough, M. P.; and Jones, D. 1978. Banded electron cyclotron harmonic instability--A direct comparison of theory and experiment. Space Sci. Rev. 22:401-417.

Scarf, F. L.; Coroniti, F. V.; Kennel, C. F.; Fredricks, R. W.; Gurnett, D. A.; and Smith, E. J. 1984. ISEE-3 wave measurements in the distant geomagnetic tail and boundary layer. Geophys. Res. Lett. 11:335-338.

Scarf, F. L.; Fredricks, R. W.; Frank, L. A.; and Neugebauer, M. 1971. Non-thermal electrons and high-frequency waves in the upstream solar wind, 1, Observations. J. Geophys. Res. 76:5162-5171.

Scarf, F. L.; Fredricks, R. W.; Kennel, C. F.; and Coroniti, F. V. 1973. Satellite studies of magnetospheric substorms on August 15, 1968. J. Geophys. Res. 78:3119-3130.

Scarf, F. L., and Gurnett, D. A. 1977. A plasma wave investigation for the Voyager mission. Space Sci. Rev. 21:289-308.

Scarf, F. L.; Gurnett, D. A.; Kurth, W. S.; and Poynter, R. L. 1979. Plasma wave turbulence at Jupiter's bow shock. Nature 280: 796-797.

Scarf, F. L.; Gurnett, D. A.; and Kurth, W. S. 1981. Plasma wave turbulence at planetary bow shocks. Nature 292:747-750.

Scarf, F. L.; Gurnett, D. A.; Kurth, W. S.; Coroniti, F. V.; Kennel, C. F.; and Poynter, R. L. 1987. Plasma wave measurements in the magnetosphere of Uranus. J. Geophys. Res. 92:15,217-15,224.

Scudder, J. D.; Mangeney, A.; Lacombe, C.; Harvey, C. C.; and Aggson, T. L. 1986a. The resolved layer of a collisionless, high β, supercritical, quasi-perpendicular shock wave, 2, Dissipative fluid electrodynamics. J. Geophys. Res. 91:11,053-11,073.

Scudder, J. D.; Mangeney, A.; Lacombe, C.; Harvey, C. C.; Wu, C. S.; and Anderson, R. R. 1986b. The resolved layer of a collisionless, high β, supercritical, quasi-perpendicular shock wave, 3, Vlasov electrodynamics. J. Geophys. Res. 91:11,075-11,097.

Selesnick, R. S., and McNutt, Jr., R. L. 1987. Voyager 2 plasma ion observations in the magnetosphere of Uranus. J. Geophys. Res., 92:15,249-15,262.

Siscoe, G. L. 1975. Particle and field environment of Uranus. Icarus 24:311-324.

Sittler, Jr., E. C.; Ogilvie, K. W.; and Selesnick, R. 1987. Survey of electrons in the Uranian magnetosphere: Voyager 2 observations. J. Geophys. Res. 92:15,263-15,281.

Stix, T. H. 1962. The Theory of Plasma Waves. New York: McGraw-Hill.

Stone, E. C.; Cooper, J. F.; Cummings, A. C.; McDonald, F. B.; Trainor, J. H.; Lal, N.; McGuire, R.; and Chenette, D. L. 1986. Energetic charged particles in the Uranian magnetosphere. Science 233:93-97.

Thorne, R. M., and Kennel, C. F. 1967. Quasi-trapped VLF propagation in the outer magnetosphere. J. Geophys. Res. 72:857-870.

Tsurutani, B. T., and Rodriguez, P. 1981. Upstream waves and particles: An overview of ISEE results. J. Geophys. Res. 86:4319-4324.

Warwick, J. W.; Evans, D. R.; Romig, J. H.; Sawyer, C. B.; Desch, M. D.; Kaiser, M. L.; Alexander, J. K.; Carr, T. D.; Staelin, D. H.; Gulkis, S.; Poynter, R. L.; Aubier, M.; Boischot, A.; Leblanc, Y.; Lecacheux, A.; Pedersen, B. M.; and Zarka, P. 1986. Voyager 2 radio observations of Uranus. Science 233:102-106.

Young, T. S. T.; Callen, J. D.; and McCune, J. E. 1973. High-frequency electrostatic waves in the magnetosphere. J. Geophys. Res. 78:1082-1099.

Zarka, P., and Lecacheux, A. 1987. Beaming of Uranian nightside kilometric radio emission and inferred source location. J. Geophys. Res. 92:15,177-15,187.

FIGURE CAPTIONS

Figure 1. An overview of the plasma wave observations at Uranus from just prior to the inbound bow shock crossing to the first of the outbound shocks (Gurnett et al., 1986). The bulk of the wave activity is in the inner magnetosphere.

Figure 2. The upstream portion of the Voyager 2 plasma wave data set showing extensive Langmuir wave activity as distant as 80 R_U.

Figure 3. A comparison of the plasma wave spectra obtained during the inbound bow shock (left panel) and one of the outbound bow shocks (right panel). The primary difference is the notch in the spectrum in the range of 30 - 100 Hz observed in the outbound shock.

Figure 4. A summary of the electrostatic Bernstein wave emissions observed by Voyager 2 at Uranus (Kurth et al., 1987). The bursty emissions above the f_c contour and below the smoothly varying radio emissions are the electostatic waves. Notice that the inner magnetospheric pass occurred at rather high magnetic latitudes (top panel), where the growth of the Bernstein waves is not expected to be large.

Figure 5. An expanded view of the Bernstein emissions observed near the magnetic equator at 11.5 R_U (Kurth et al., 1987). Notice the bursty nature of the waves and the broad frequency extent. This spectrum is likely composed of narrowband emissions between the first three or four harmonics of the electron cyclotron frequency.

Figure 6. An overview of the extensive occurrence of whistler mode waves, seen here below the f_c contour (Gurnett et al., 1986).

Figure 7. A series of 10-second snapshots of the detailed frequency-time character of the whistler mode emissions represented in Figure 6 (Gurnett et al., 1986). Panel B shows an example of chorus growing out of the top of the hiss band and Panel D shows the very bursty and as yet unidentified emissions near 1930 SCET where the whistler band is interupted (see Figure 6).

Figure 8. A 0.6-second average of the wave spectrum from the hiss band shown in Panel F of Figure 7 showing the detailed form of the hiss band (Coroniti et al., 1987). Notice the extended bandwidth of the emission.

Figure 9. A comparison of the intensity of the whistler mode emissions and fluxes of energetic electrons from the LECP investigation (Coroniti et al., 1987). The peak whistler mode intensities correlate well with the peak fluxes of the energetic electrons.

Figure 10. The model electron distribution used by Coroniti et al. (1987) (dashed line) for the whistler mode interaction calculation (Coroniti et al., 1987).

Figure 11. The results of the fitted gain calculation (dots) compared to the measured gain obtained from the Voyager 2 power spectrum (Coroniti et al., 1987).

Figure 12. A comparison of the scattering time, T_s, calculated from the bounce-averaged diffusion coefficient and T_{min}, the minimum precipitation lifetime (Coroniti et al., 1987). When the scattering time is less than T_{min} the electrons are precipitating at or near the strong diffusion limit.

Figure 13. An overview of the low frequency waves observed in the magnetotail of Uranus from Kurth et al. (1988). Notice that the activity is confine to frequencies below f_c and are observed before the first and after the second neutral sheet crossing.

Figure 14. Typical spectra of the waves observed in the magnetotail (Kurth et al., 1988). The spectra are reminiscent of broadband electrostatic waves in the terrestrial magnetosphere.

Figure 15. A schematic drawing of the Uranian plasma sheet taken from Mauk et al. (1987) showing the locations of the plasma wave activity (from Kurth et al., 1988). Notice the waves are confined to the southern magnetic hemisphere.

Figure 16. A schematic summary of the locations of various plasma wave phenomena detected in and near the magnetosphere of Uranus. Note that the limited spatial coverage of the Voyager 2 trajectory limits the accuracy of such a graphic.

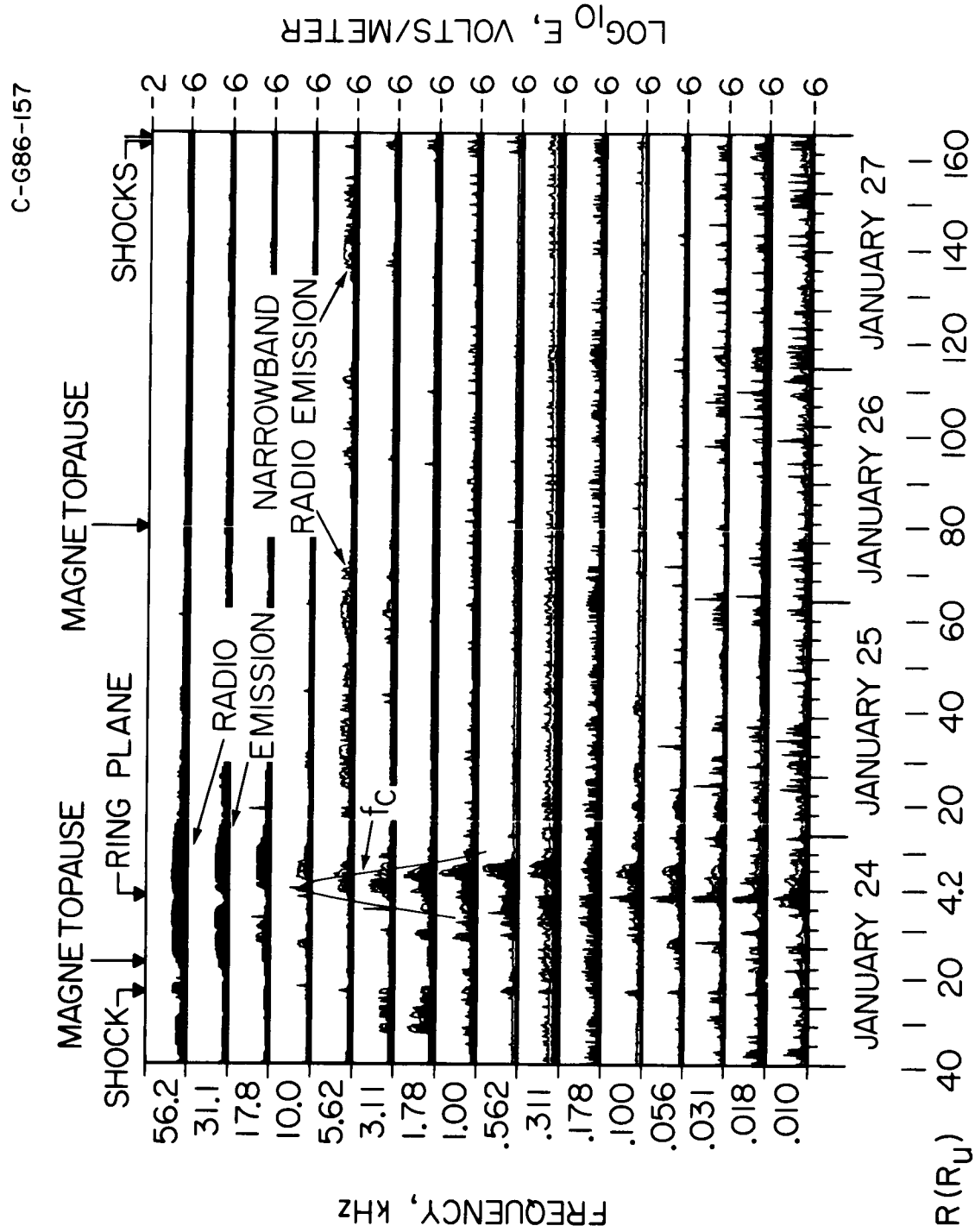

Figure 1

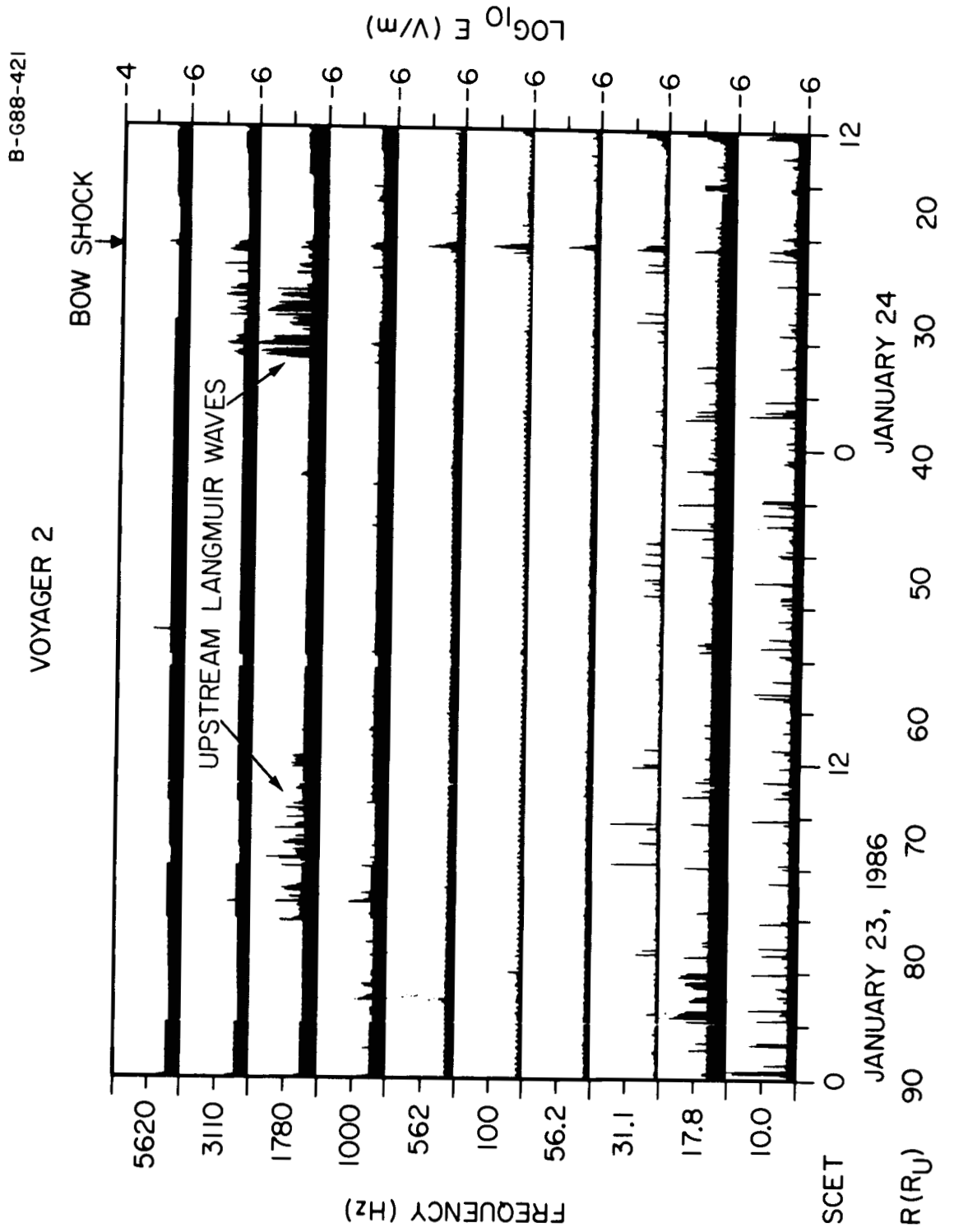

Figure 2

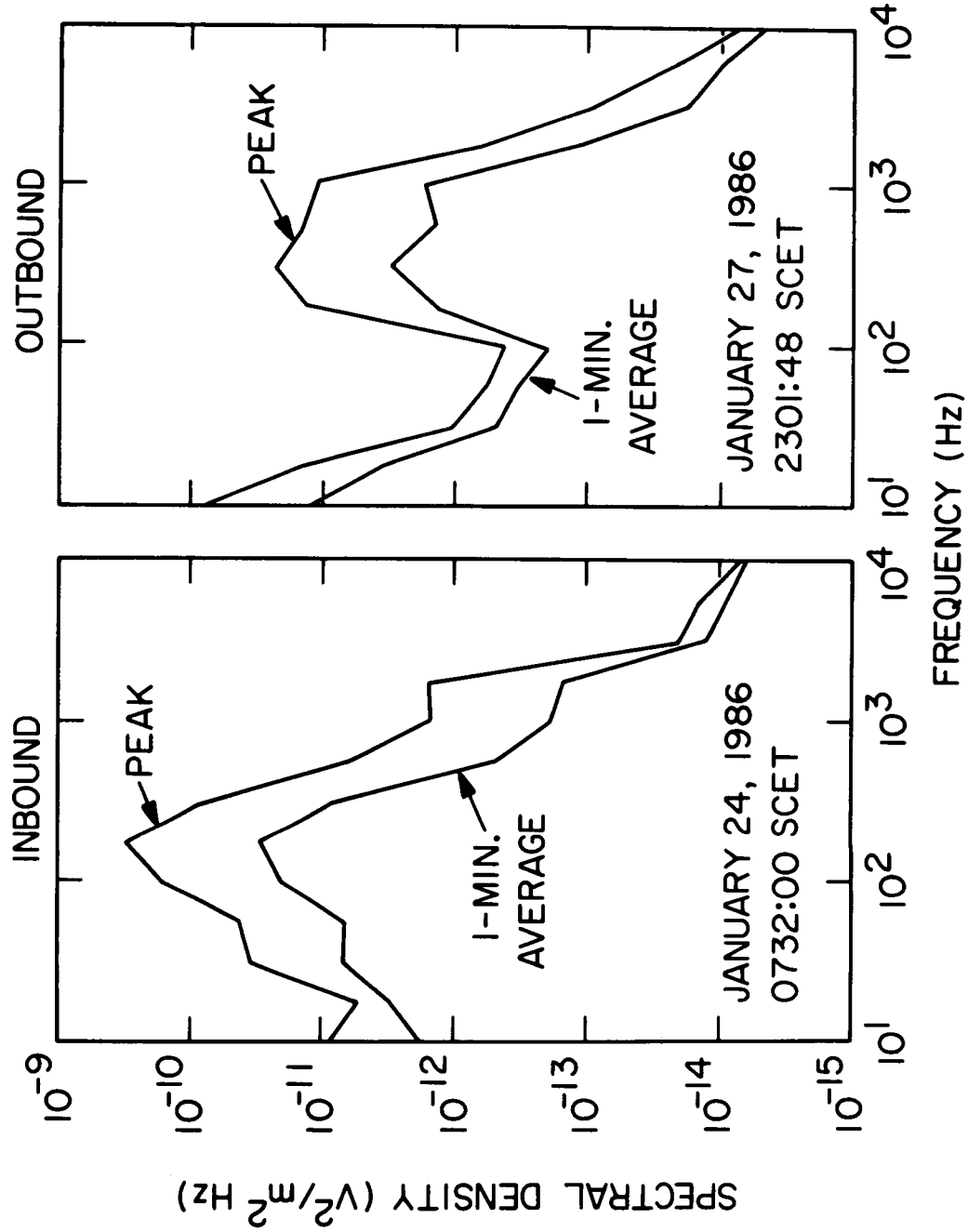
A-G88-425
VOYAGER 2
INBOUND
OUTBOUND
PEAK
1-MIN. AVERAGE
JANUARY 24, 1986
0732:00 SCET
JANUARY 27, 1986
2301:48 SCET
SPECTRAL DENSITY (V²/m² Hz)
FREQUENCY (Hz)
10⁻⁹
10⁻¹⁰
10⁻¹¹
10⁻¹²
10⁻¹³
10⁻¹⁴
10⁻¹⁵
10¹
10²
10³
10⁴

Figure 3

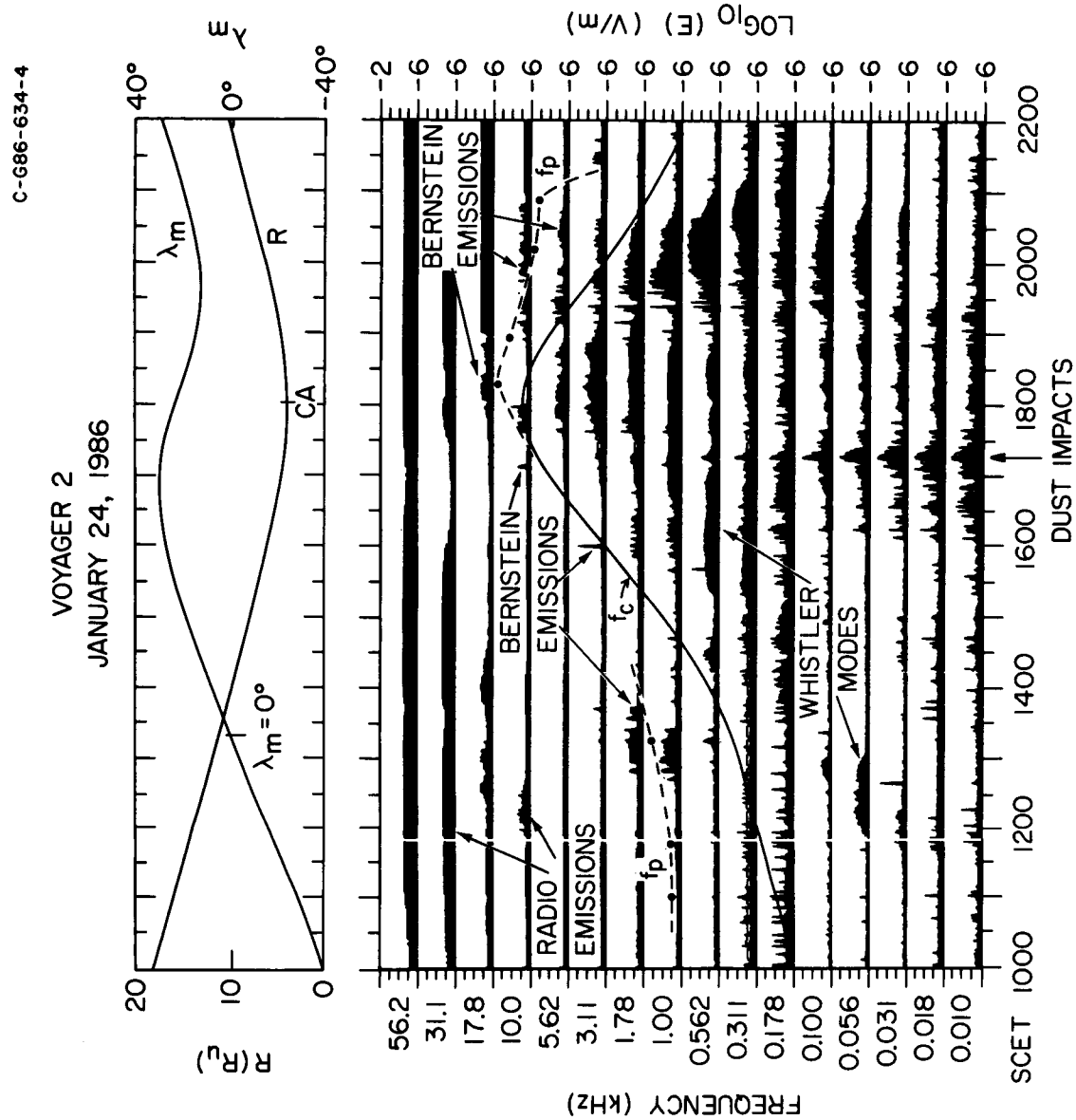

Figure 4

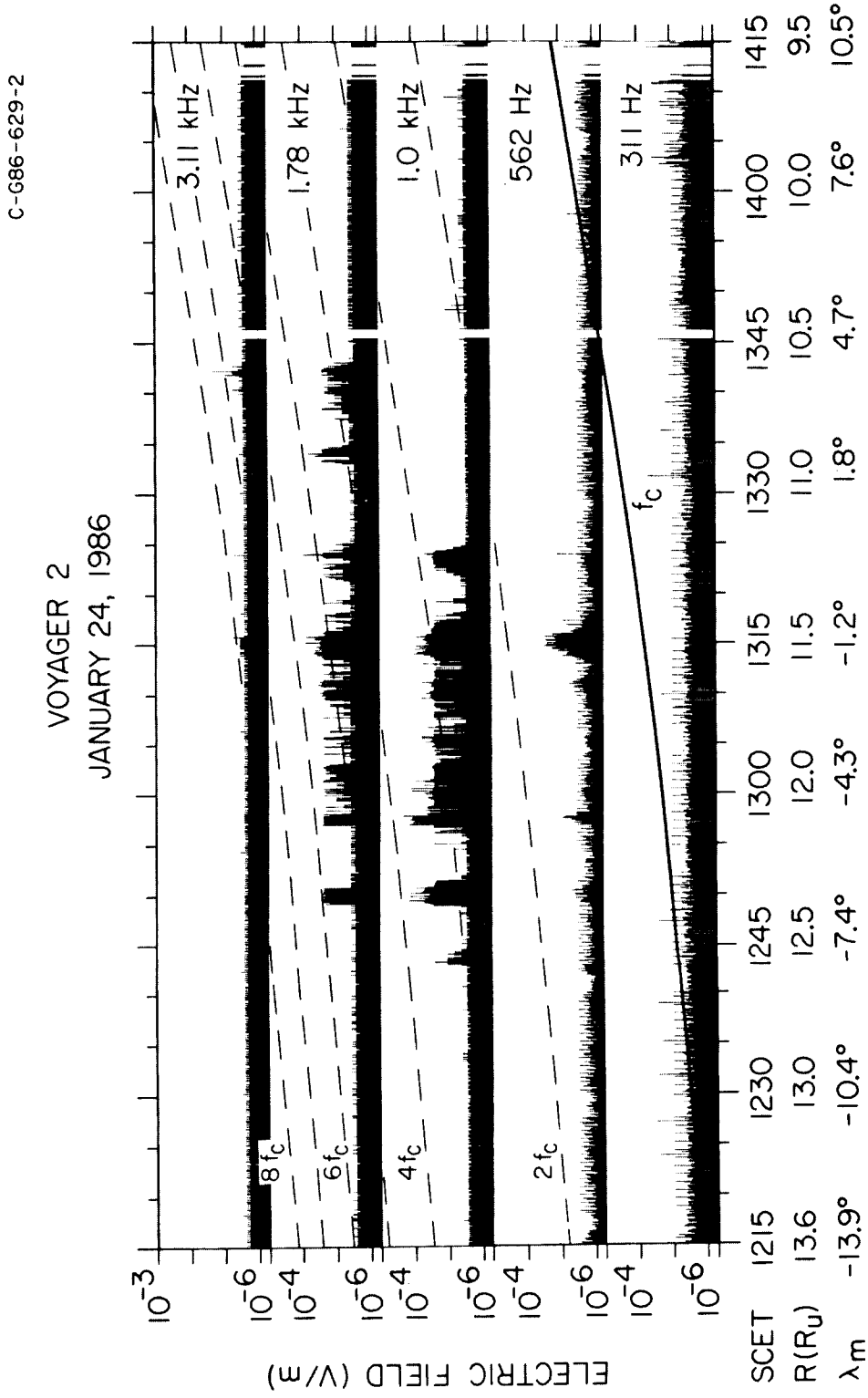

Figure 5

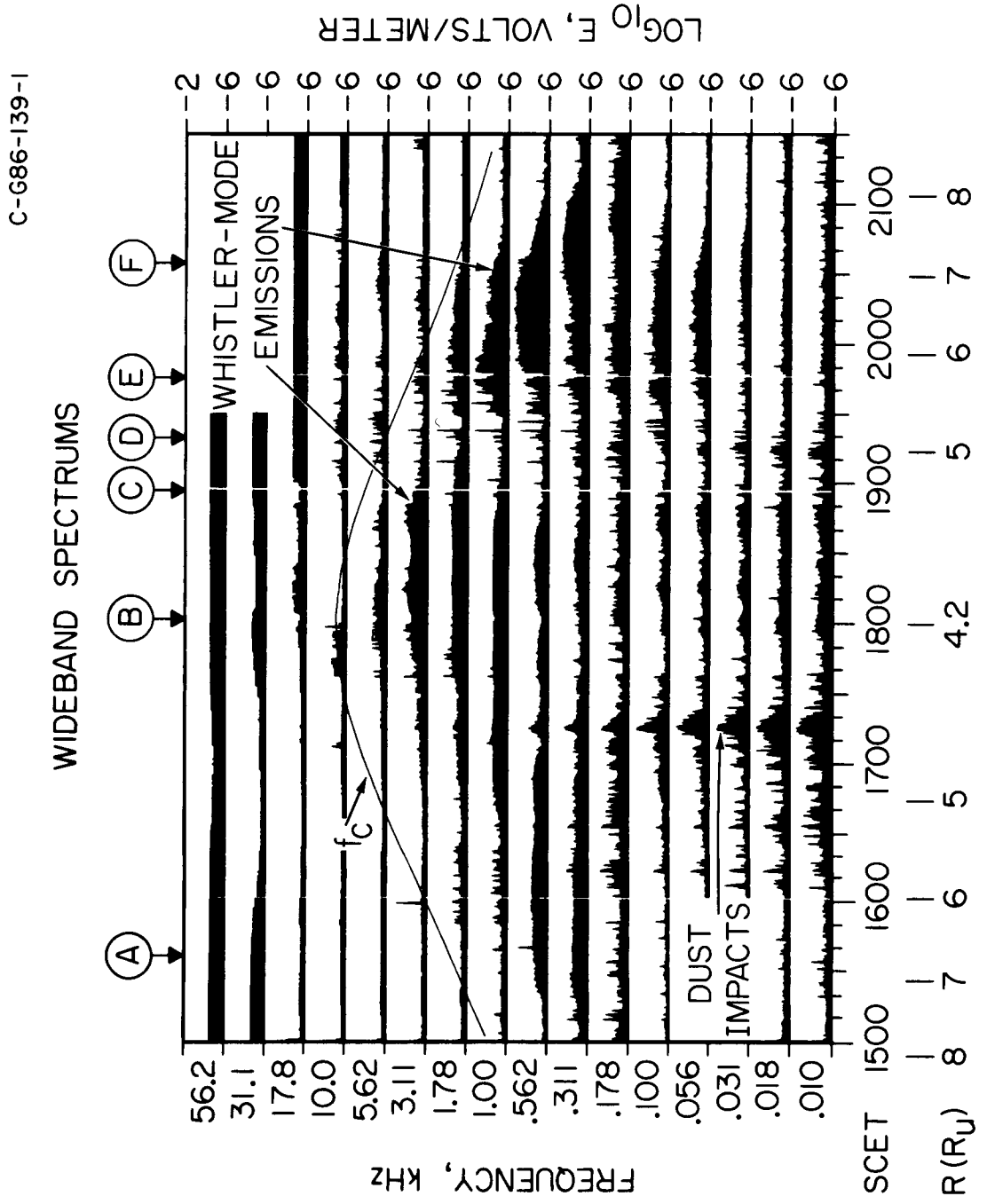

Figure 6

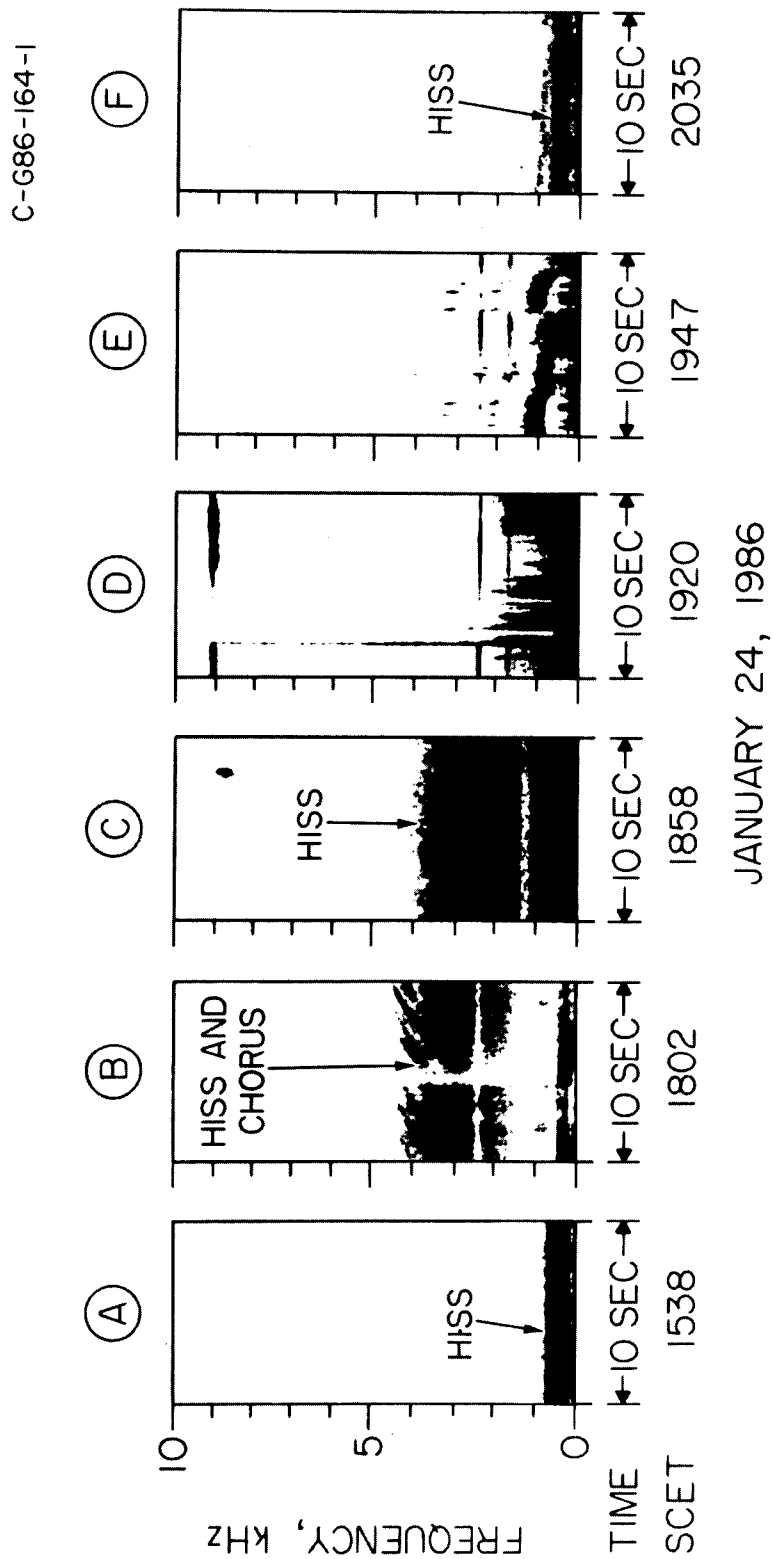

Figure 7

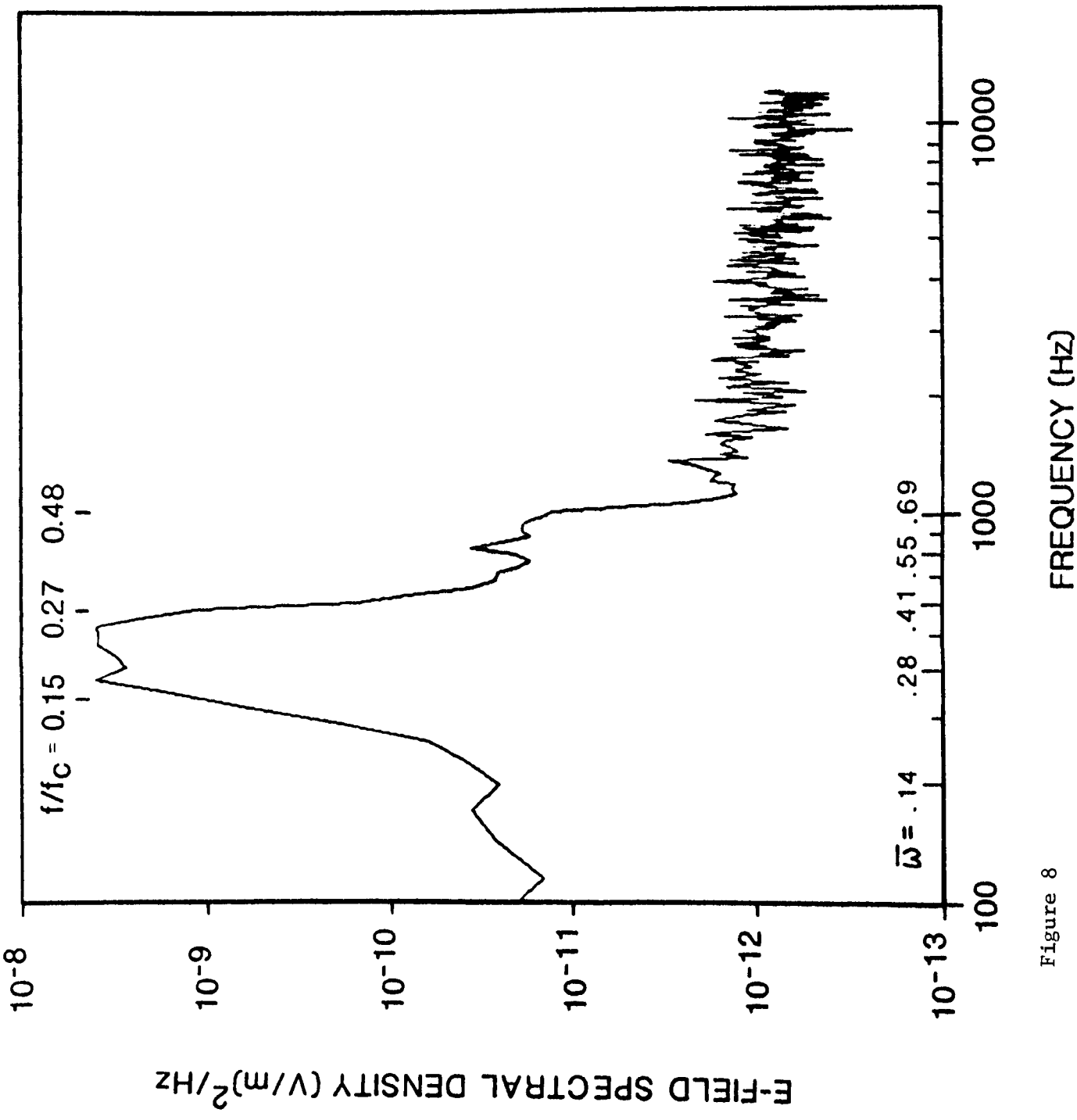
VOYAGER-2, 2035 SCET, JANUARY 24, 1986
f/fc = 0.15 0.27 0.48
ω̄ = .14 .28 .41 .55 .69
E-FIELD SPECTRAL DENSITY (V/m)²/Hz
FREQUENCY (Hz)
10⁻⁸
10⁻⁹
10⁻¹⁰
10⁻¹¹
10⁻¹²
10⁻¹³
100
1000
10000
86-82

Figure 8

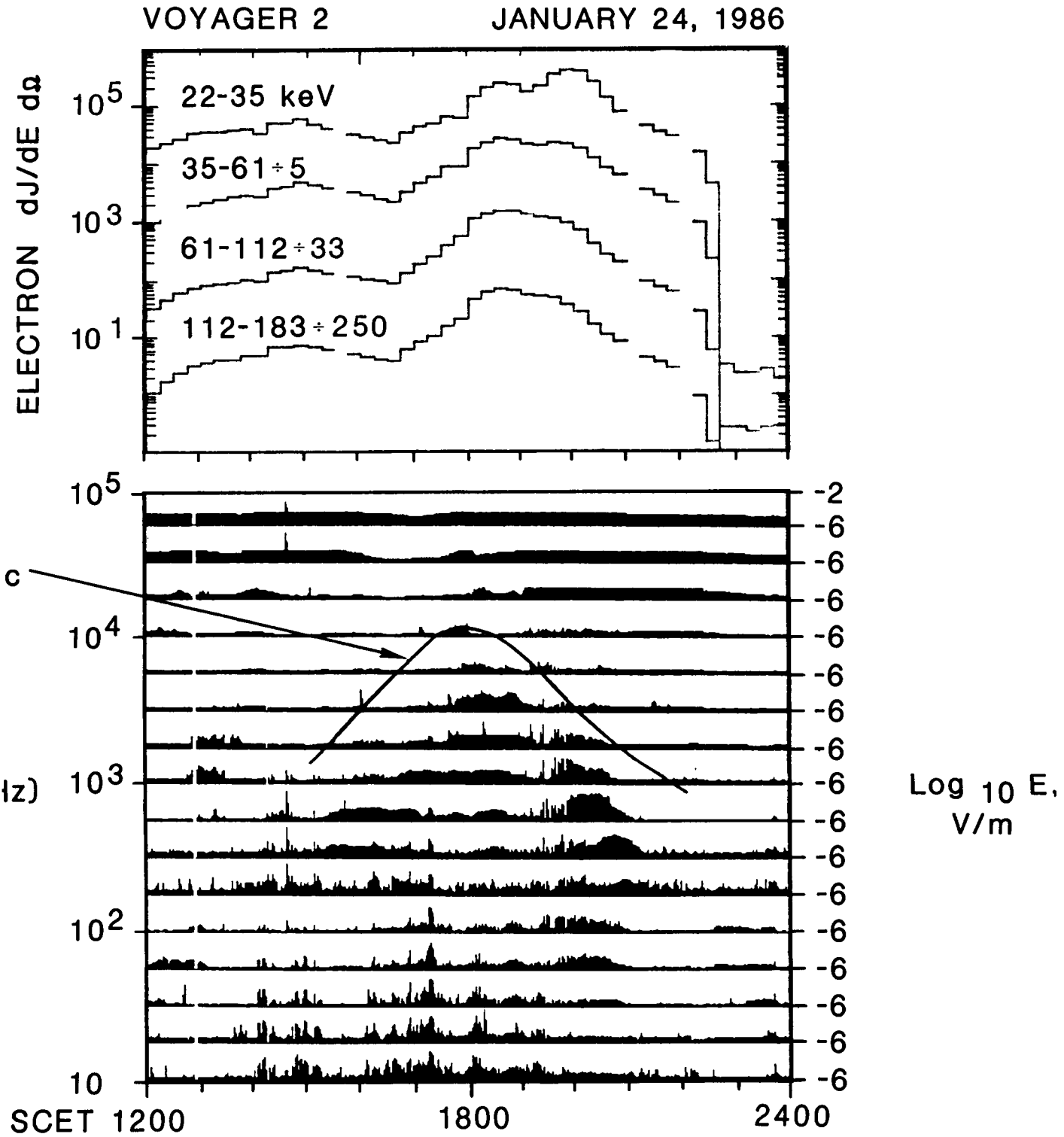

Figure 9

86-84

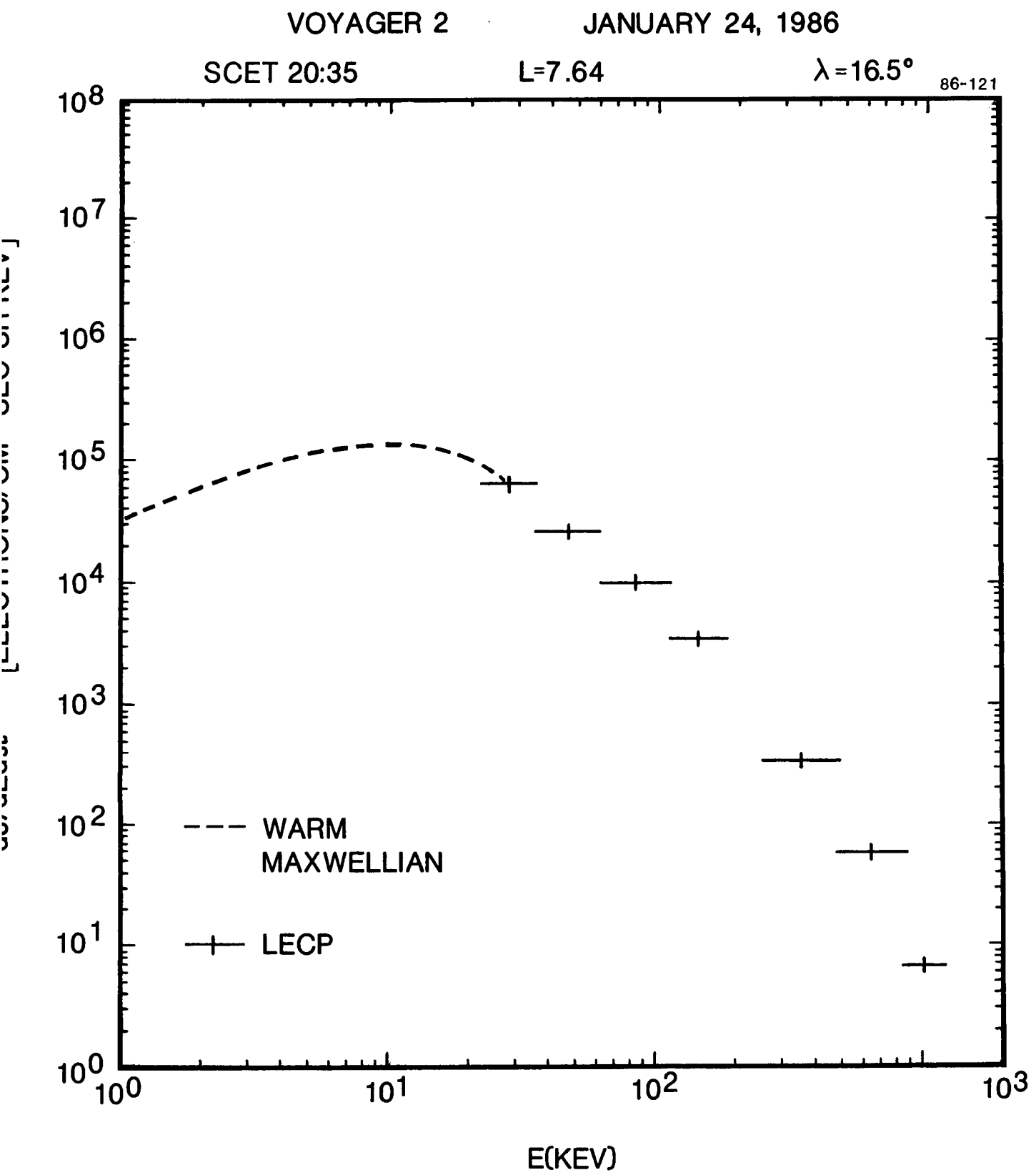
VOYAGER 2
JANUARY 24, 1986
SCET 20:35
L=7.64
λ=16.5°
86-121
10^8
10^7
10^6
10^5
10^4
10^3
10^2
10^1
10^0
WARM
MAXWELLIAN
LECP
10^0
10^1
10^2
10^3
E(KEV)

Figure 10

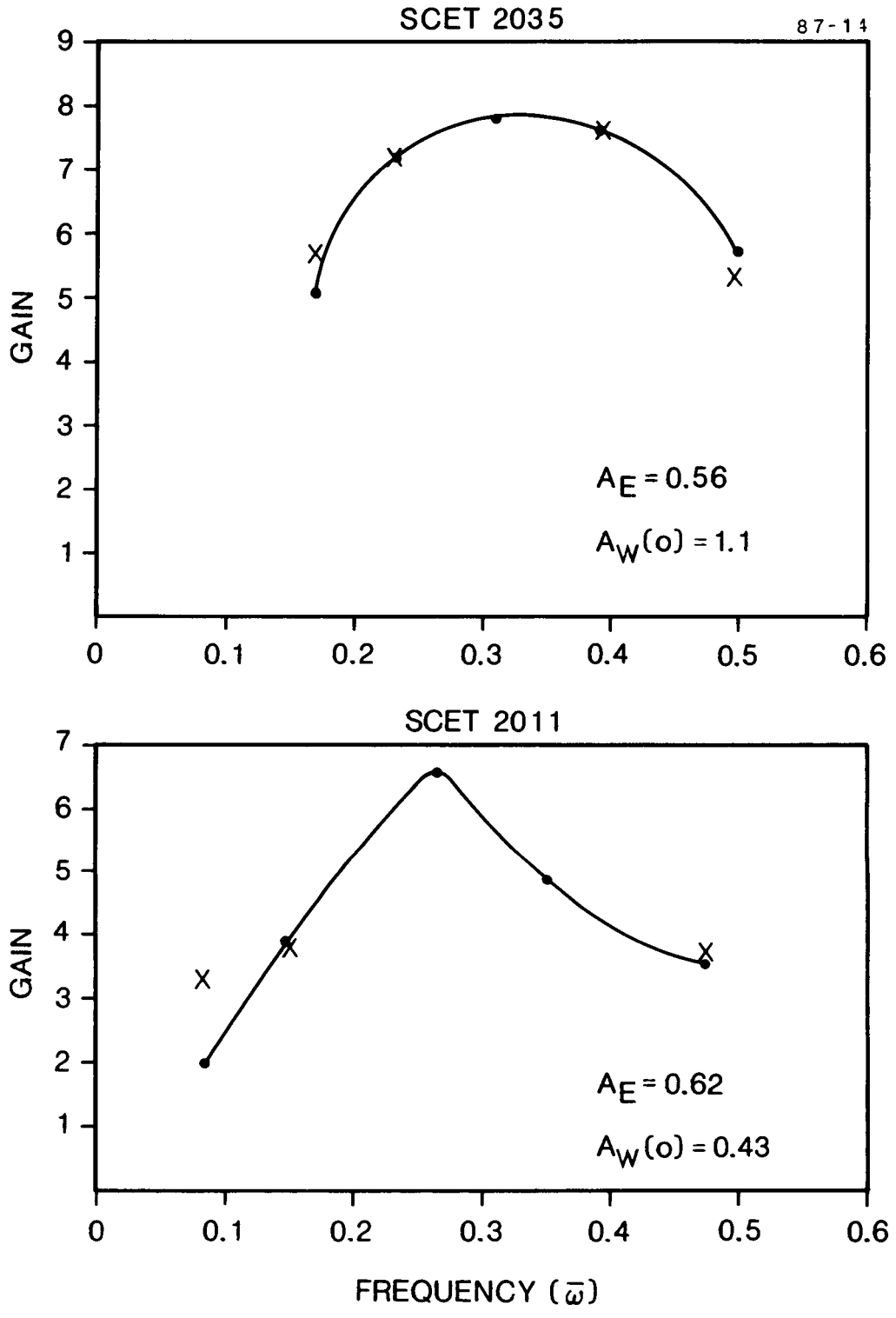
SCET 2035
87-14
GAIN
$A_E = 0.56$
$A_W(o) = 1.1$
SCET 2011
GAIN
$A_E = 0.62$
$A_W(o) = 0.43$
FREQUENCY ($\bar{\omega}$)

Figure 11

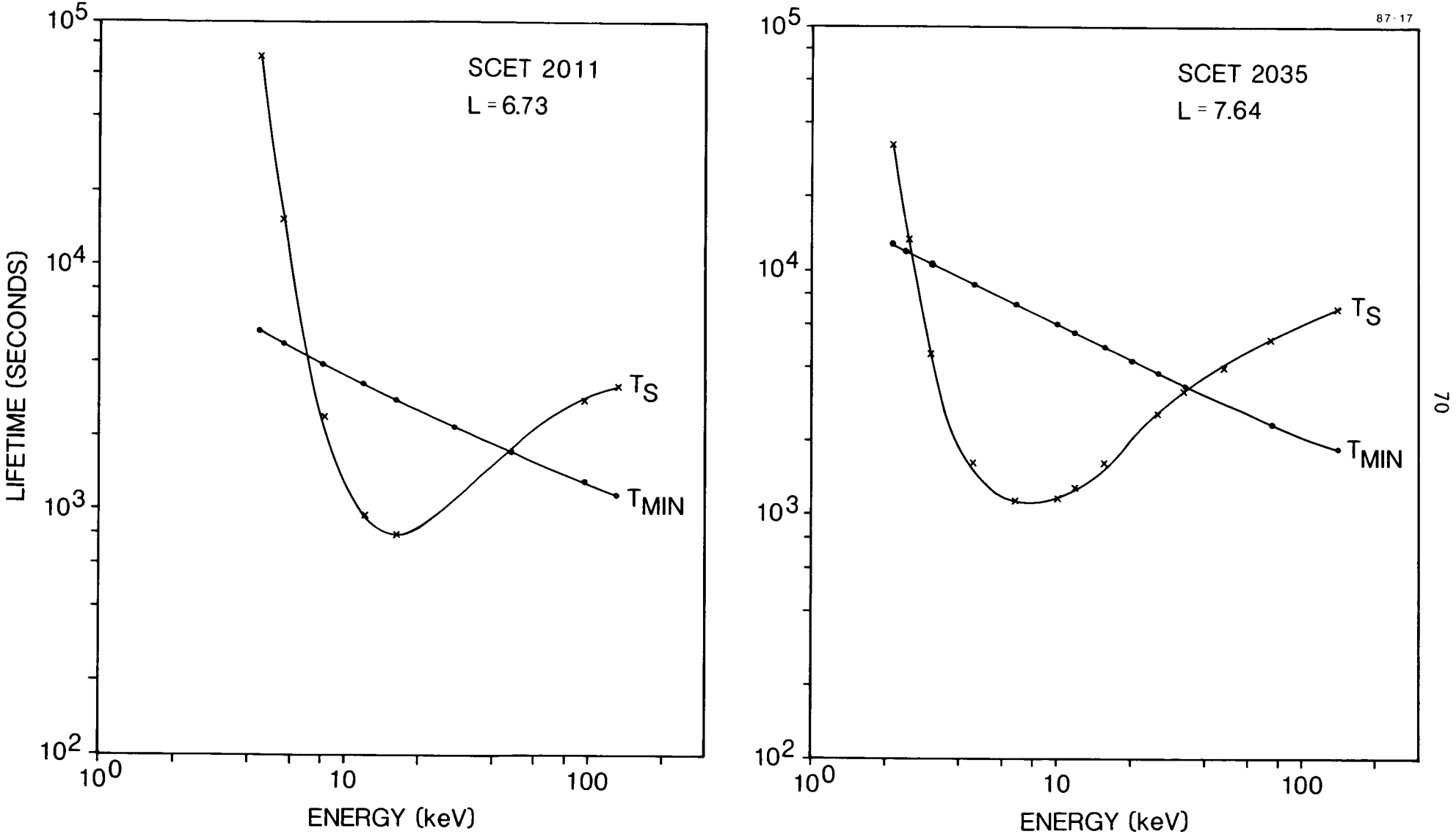
LIFETIME (SECONDS)
10^5
10^4
10^3
10^2
SCET 2011
L = 6.73
T_S
T_{MIN}
10^0
10
100
ENERGY (keV)
87-17
SCET 2035
L = 7.64
T_S
T_{MIN}
ENERGY (keV)
70

Figure 12

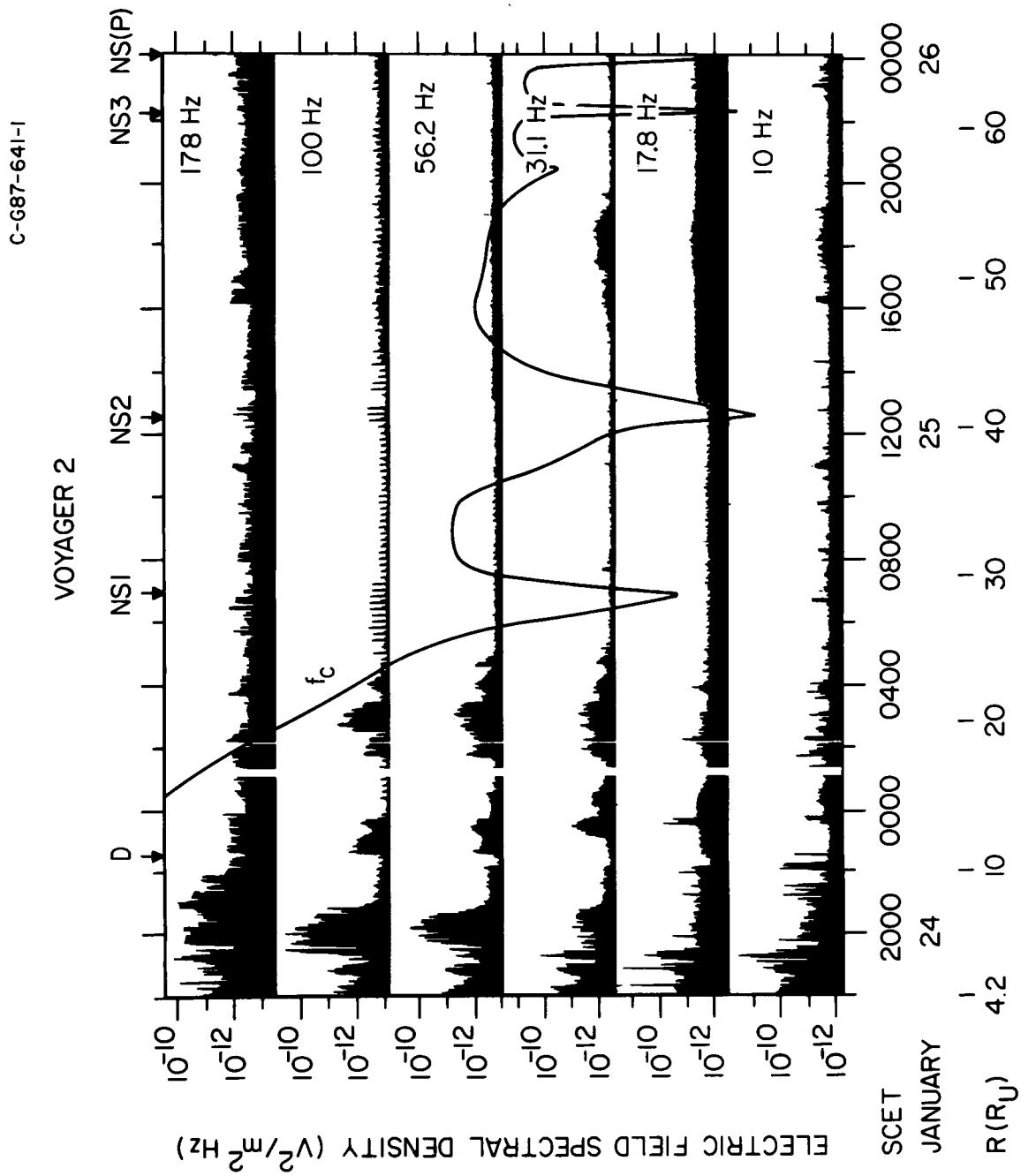

Figure 13

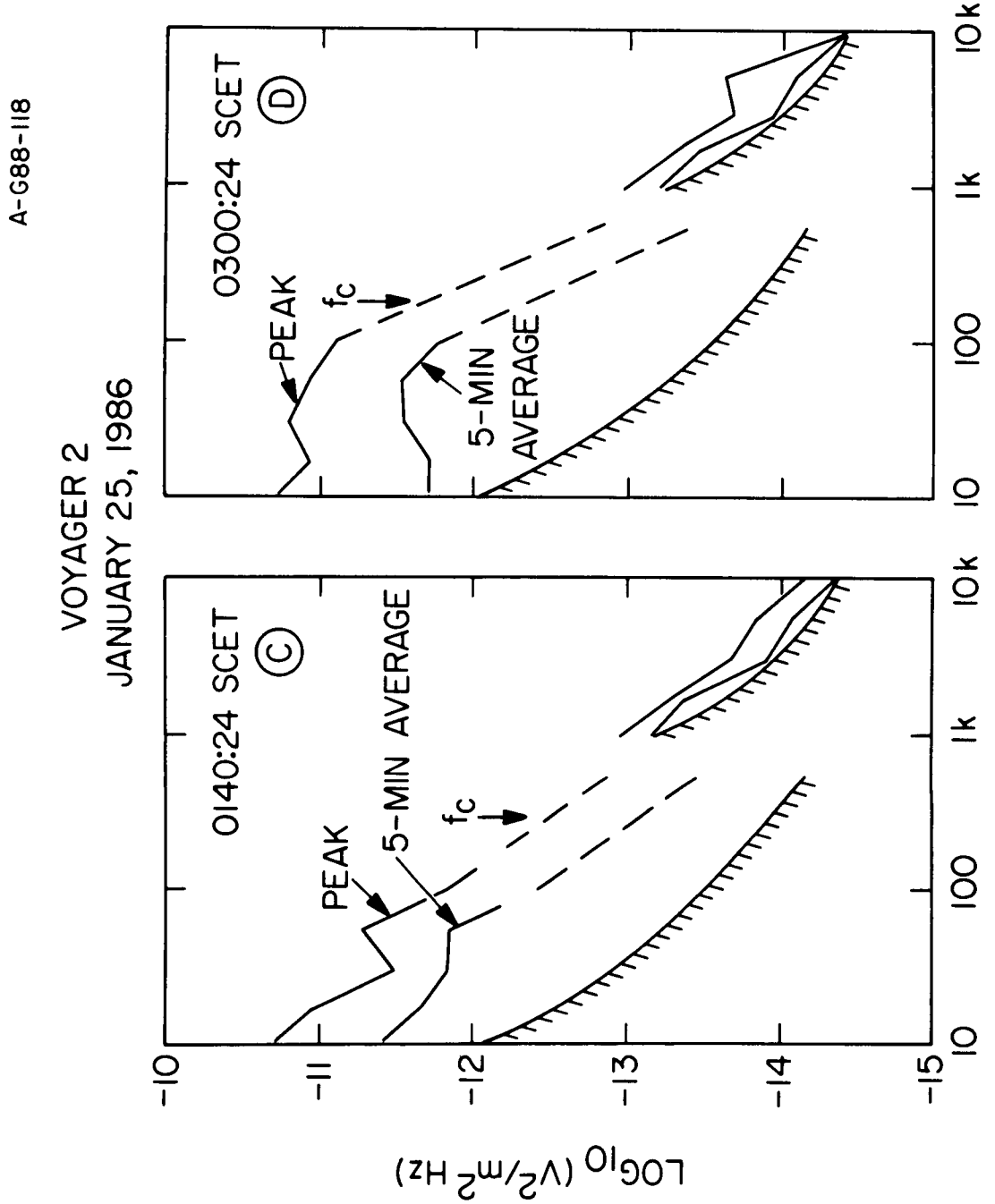
A-G88-118
VOYAGER 2
JANUARY 25, 1986
0140:24 SCET
C
PEAK
5-MIN AVERAGE
f_c
0300:24 SCET
D
PEAK
f_c
5-MIN AVERAGE
$\log_{10}$ (V^2/m^2 Hz)
-10
-11
-12
-13
-14
-15
10
100
1k
10k
FREQUENCY (Hz)

Figure 14

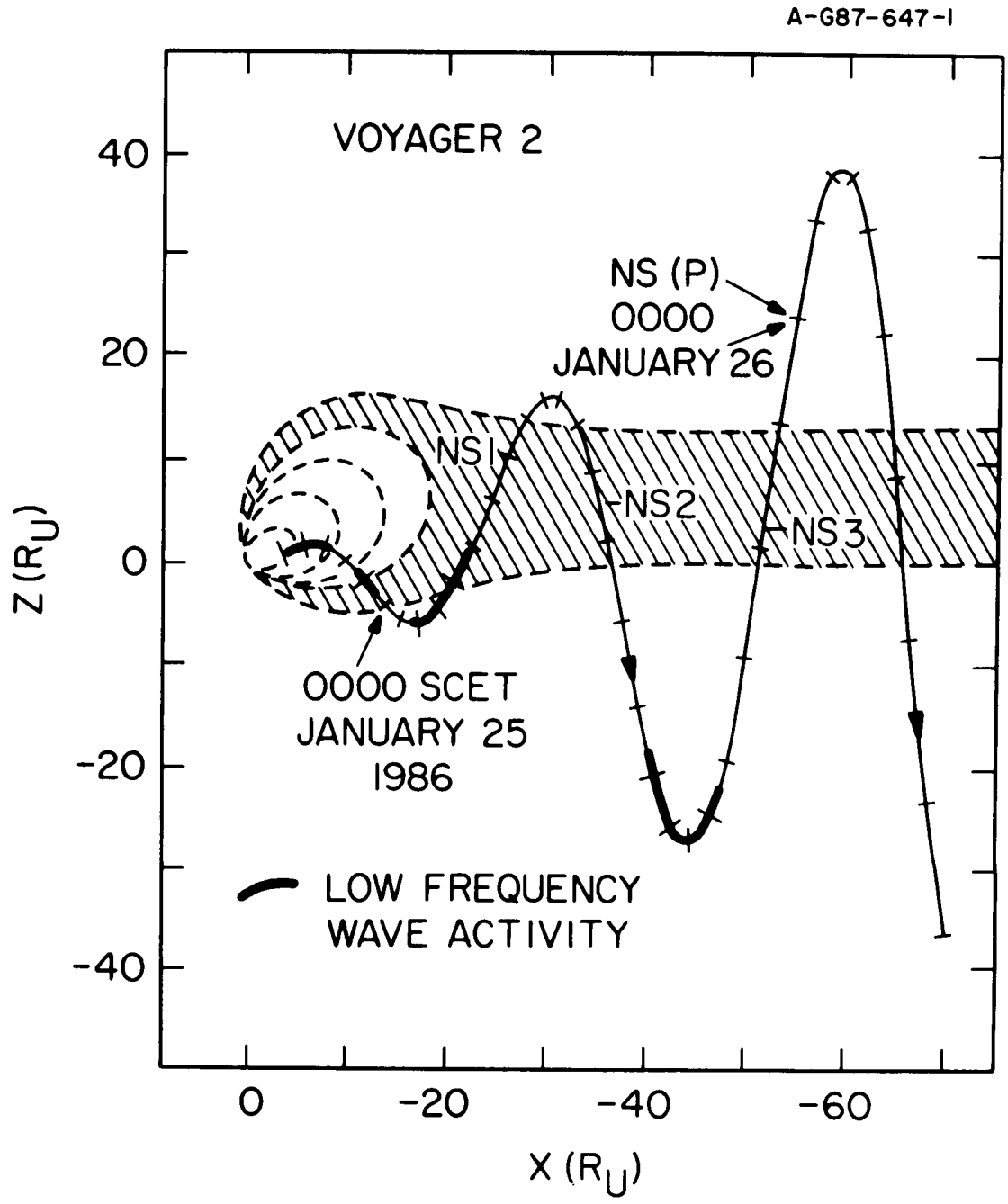
A-G87-647-I
VOYAGER 2
NS (P)
0000
JANUARY 26
NS1
NS2
NS3
0000 SCET
JANUARY 25
1986
LOW FREQUENCY
WAVE ACTIVITY
40
20
0
-20
-40
Z (R_U)
0
-20
-40
-60
X (R_U)

Figure 15

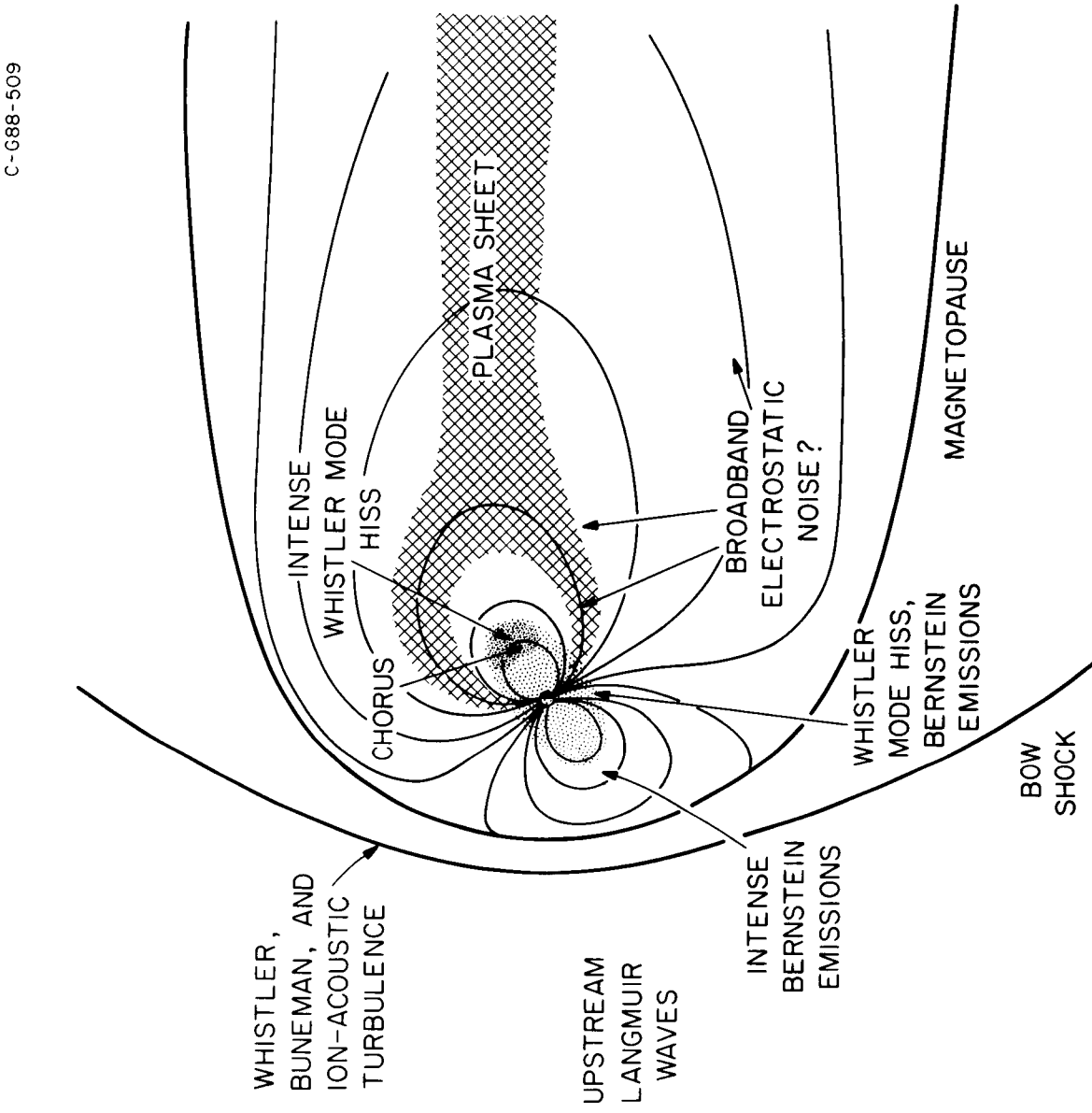

Figure 16